Intelligent nonsingular terminal sliding-mode control via perturbed fuzzy neural network

Chun-Fei Hsu[1], Tsu-Tian Lee[1], and Kazuo Tanaka[2]
[1] Department of Electrical Engineering, Tamkang University,
No. 151, Yingzhuan Rd., Tamsui Dist., New Taipei City 25137, Taiwan
E-mail: fei@ee.tku.edu.tw; ttlee@ee.tku.edu.tw
[2] Department of Mechanical Engineering and Intelligent Systems, University of Electro-Communications, Tokyo, Japan
E-mail: ktanaka@mce.uec.ac.jp

Abstract

In this paper, an intelligent nonsingular terminal sliding-mode control (INTSMC) system, which is composed of a terminal neural controller and a robust compensator, is proposed for an unknown nonlinear system. The terminal neural controller including a perturbed fuzzy neural network (PFNN) is the main controller and the robust compensator is designed to eliminate the effect of the approximation error introduced by the PFNN upon the system stability. The PFNN is used to approximate an unknown nonlinear term of the system dynamics and perturbed asymmetric membership functions are used to handle rule uncertainties when it is hard to exactly determine the grade of membership functions. In additional, Lyapunov stability theory is used to discuss the parameter learning and system stability of the INTSMC system. Finally, the proposed INTSMC system is applied to an inverted pendulum and a voice coil motor actuator. The simulation and experimental results show that the proposed INTSMC system can achieve favorable tracking performance and is robust against parameter variations in the plant.

Keywords: Intelligent control; Sliding-mode control; Fuzzy neural network; Perturbed membership function.

1. Introduction

In the last 40 years, the sliding-mode control (SMC) system has been successfully applied to handle several practical control problems in face of system uncertainties and time-varying disturbances (Nayeripour et al., 2011; Zhang et al., 2014). It is known that the chattering problem is one of the most critical handicaps for applying the SMC system to real applications. A solution to this problem is the high-order SMC system (Gennaro et al., 2014; Na et al., 2013). The actual control signal was obtained after integrating the discontinuous derivative control law; however, the main problem of the high-order SMC is the increasing information demand. Meanwhile, Yang et al. (2014) proposed a continuous dynamic SMC system to drive the states to the dynamic sliding surface. Though the level of the chattering phenomenon can be reduced; however, the design procedure is overly complex.

Motivated by the previous discussions, the most commonly used sliding surface is a hyperplane-based sliding surface. The SMC system using the hyperplane-based sliding surface cannot guarantee the convergence in finite time. To attack this problem, a terminal sliding-mode control (TSMC) is presented by introducing a nonlinear item into the sliding mode which offers some superior properties such as fast and better control precision (Chen et al., 2012; Li et al., 2013; Tan et al., 2010; Yu et al., 2005). The states of the TSMC system can guarantee converging to the origin in finite time. Though the TSMC provides fast convergence and high precision control, there are two disadvantages in the TSMC system. One is the singularity point problem and the other is the requirement of system dynamics. To resolve the singularity problem, a nonsingular terminal sliding-mode control (NTSMC) system was proposed (Feng et al. 2013; Komurcugil, 2013; Yang et al., 2013). Though favorable control performance can be achieved by both of TSMC and NTSMC systems, not only the chattering phenomenon cannot be avoided but also these schemes required detailed system models.

Some researchers focus on intelligent NTSMC (INTSMC) approaches to attack the requirement of the system dynamics (Chen and Lin, 2011; Lin, 2006; Lin et al., 2012). Lin (2006) used a fuzzy wavelet network to accurately approximate the unknown dynamics of robotic systems. Though the tracking performance can be guaranteed by Lyapunov stability theory, a conservative switching control law was constructed to cause damage to actuators. The chattering problem is one of the most critical handicaps for applying the INTSMC system to real applications. Chen and Lin (2011) proposed a recurrent Hermite neural network uncertainty estimator to improve the control performance and increase the robustness of the control system. However, the algorithm supposed that the approximation error is constant but this is not true due to the approximated function is a function of the states. Lin et al. (2012) developed an interval type-2 recurrent fuzzy neural network to approximate a lumped uncertainty. However, the type-reduction operation of the interval type-2 recurrent fuzzy neural network results in heavy computational loading. It is unsuitable for real-time control applications.

Though the INTSMC system can achieve favorable control performance, the approximation error introduced by the used neural networks may cause instability of the control system. Thus, an extra compensator, such as the switching compensator (Mon and Lin, 2012) and the supervisory compensator (Chen and Hsu, 2010), should be used. These compensators result in the chattering phenomena so as to cause damage to actuators or plants. Zhao et al. (2011) proposed a low-pass filtering for chattering reduction; however, a trade-off problem between chattering phenomenon and control accuracy arises. A L_2 compensator was proposed (Hsu, 2012; Lee and Li, 2012). The control input may lead to a large control signal as the specified attenuation level was chosen small. A smooth compensator was proposed to achieve the uniformly ultimately bound stability of the control system without occurring chattering phenomena (Kim and Calise, 2007; Lin and Li, 2013; Na et al., 2013).

When the approximator error is large, the smooth compensator cannot improve the convergent speed of tracking error due to its control gain is fix.

It is known that the type-1 fuzzy sets are unable to directly handle the rule uncertainties. To attack this problem, several studies on the theory of type-2 fuzzy systems have been conducted (Castillo and Melin, 2012; Lou and Dong, 2012; Mendel, 2001). Type-2 fuzzy systems make it possible to model and minimize the effects of uncertainties that cannot be directly modeled by type-1 fuzzy systems. Though interval type-2 fuzzy systems are useful in handling uncertainties, the problem of how to design interval type-2 fuzzy systems remains an unsolved problem. To address this problem, several interval type-2 fuzzy neural networks (T2FNNs) were proposed based on gradient-descent-learning algorithms (Abiyev and Kaynak, 2010; Chang and Chan, 2014; Kayacan et al., 2012 and 2015). The interval T2FNNs use a typical type reduction operation, namely the Karnik-Mendel iterative procedure, to find the extended output. The type reduction operation is complex and time consuming, especially for hardware implementation. A simplified type reduction operation was proposed to reduce the hardware implementation cost (Juang and Chen, 2013 and 2014; Juang and Juang, 2014) proposed.

Contributions of this paper are twofold. First, a perturbed fuzzy neural network (PFNN) using a perturbed asymmetric membership function is proposed. The perturbed functions possess the ability of handling rule uncertainties with a simplified computation complexity. Unlike interval T2FNN, the PFNN does not require the time-consuming type reduction operation. The proposed online parameter learning ability makes it feasible for online approximating an unknown nonlinear term of the system dynamics. Second, an intelligent nonsingular terminal sliding-mode control (INTSMC) system is proposed for an unknown nonlinear system. The design contains two parts. One is the design of terminal neural controller and the other is the design of robust compensator upon the system stability. The

robust compensator which is based on the choice of an exponential term that adapts to the variation of the system states is proposed. Thus, the control chattering occurred in TSMC and NTSMC can be alleviated. Further, the proposed INTSMC system is applied to an inverted pendulum and a voice coil motor (VCM) actuator to verify its effectiveness.

2. Problem formulation

Consider an *n*-th order nonlinear system as

$$x^{(n)} = f(\mathbf{x}) + g(\mathbf{x})u \tag{1}$$

where $\mathbf{x} = [x, \dot{x}, ..., x^{(n-1)}]^T$ is the state vector, $f(\mathbf{x})$ and $g(\mathbf{x})$ are the system dynamics, and u is the control input. Without losing generality, it is assumed that $g(\mathbf{x}) > 0$ for all time. The control objective is to find a control law so that the state vector $\mathbf{x}$ can track a command vector $\mathbf{x}_c = [x_c, \dot{x}_c, ..., x_c^{(n-1)}]^T$ closely. To achieve this control objective, define a tracking error vector as

$$\mathbf{e} = \mathbf{x} - \mathbf{x}_c = [e, \dot{e}, ..., e^{(n-1)}]^T \tag{2}$$

where $e = x - x_c$. Substituting (1) into (2) yields

$$e^{(n)} = u + z(\mathbf{x}) \tag{3}$$

where the nonlinear term $z(\mathbf{x})$ is defined as $z(\mathbf{x}) = -x_c^{(n)} + (1 - \frac{1}{g(\mathbf{x})})x^{(n)} + \frac{f(\mathbf{x})}{g(\mathbf{x})}$. If the system uncertainties occur, i.e., parameters of the system deviate from its nominal values, the error dynamic equation can be modified as

$$e^{(n)} = u + z_n(\mathbf{x}) + \Delta z(\mathbf{x}) \tag{4}$$

where $z_n(\mathbf{x})$ is the nominal behavior of nonlinear term $z(\mathbf{x})$ and $\Delta z(\mathbf{x})$ denotes the system uncertainties. It is assumed to be bounded by $|\Delta z(\mathbf{x})| \le Z$ where Z is a positive constant.

In this study, a nonsingular terminal sliding surface is designed as Feng et al. (2013)

$$s_i = s_{i-1} + \frac{1}{\lambda_i}\dot{s}_{i-1}^{\frac{p_i}{q_i}}, \text{ for } i = 1,2,...,n-1 \tag{5}$$

where $s_0 = e$, λ_i is designed positive constant and p_i and q_i are positive odd integers which should satisfy the condition $q_i < p_i < 2q_i$. If a controller can guarantee that the system state approaches the nonsingular terminal sliding surface $s_i = 0$ in finite time and confines the state on the sliding surface, $s_{i-1} = 0$ can be achieved as Feng et al. (2013). When the nonsingular terminal sliding surface is reached within limited time t_r, the system dynamic can be determined by the following nonlinear differential equation

$$\dot{s}_{i-1} = -\lambda_i s_{i-1}^{\frac{q_i}{p_i}} \tag{6}$$

Then, a finite time t_s is taken to travel from $s_{i-1}\big|_{t=t_r} \neq 0$ to $s_{i-1}\big|_{t=t_r+t_s} = 0$. So on so forth, finally $s_1 = 0$ and $s_0 = 0$ (that is $e = 0$) will converge to zero within a limited time.

Assuming that the nominal system dynamic $z_n(\mathbf{x})$ is known, there exists an NTSMC system as Feng et al. (2013)

$$u_{smc} = -z_n(\mathbf{x}) - \sum_{i=1}^{n-1} \lambda_i \frac{q_i}{p_i} \frac{d^{n-i} s_{i-2}}{dt^{n-i}}^{2-\frac{p_i}{q_i}} - Z\,\mathrm{sgn}(s_{n-1}) \tag{7}$$

where $\mathrm{sgn}(\cdot)$ is a sign function. It is obvious that the term $\lambda_i \frac{q_i}{p_i} \frac{d^{n-i} s_{i-2}}{dt^{n-i}}^{2-\frac{p_i}{q_i}}$ in (7) will not result in the negative power as lone as the condition $q_i < p_i < 2q_i$ holds for $i = 1,2,...,n-1$. Differentiating (5) with respect to time and using the control law $u = u_{smc}$, we can obtain that

$$\begin{aligned} \dot{s}_{n-1} &= \dot{s}_{n-2} + \frac{1}{\lambda_{n-1}} \frac{p_{n-1}}{q_{n-1}} \dot{s}_{n-2}^{\frac{p_{n-1}}{q_{n-1}}-1} \dot{s}_{n-2} \\ &= \delta_{n-2}[\Delta z(\mathbf{x}) - Z\,\mathrm{sgn}(s_{n-1})] \end{aligned} \tag{8}$$

where $\delta_{n-2} = \frac{1}{\lambda_{n-1}} \frac{p_{n-1}}{q_{n-1}} \dot{s}_{n-2}^{\frac{p_{n-1}}{q_{n-1}}-1}$. Since p_{n-1} and q_{n-1} are both positive odd integers and $1 < \frac{p_{n-1}}{q_{n-1}} < 2$, there is $\dot{s}_{n-2}^{\frac{p_{n-1}}{q_{n-1}}-1} > 0$ and $\delta_{n-2} > 0$ for $\dot{s}_{n-2} \neq 0$. To guarantee the stability of the NTSMC system, consider the candidate Lyapunov function in the following form as

$$V_1(t) = \frac{1}{2} s_{n-1}^{\ 2} \tag{9}$$

Differentiating (9) with respect to time and using (8) yields

$$\begin{aligned} \dot{V}_1(t) &= s_{n-1}\dot{s}_{n-1} \\ &= \delta_{n-2}[\Delta z(\mathbf{x}) s_{n-1} - Z|s_{n-1}|] \\ &\leq \delta_{n-2}[|\Delta z(\mathbf{x})||s_{n-1}| - Z|s_{n-1}|] \\ &= -\delta_{n-2}(Z - |\Delta z(\mathbf{x})|)|s_{n-1}| \leq 0 \end{aligned} \tag{10}$$

The stability of the NTSMC system can be guaranteed in the sense of the Lyapunov theorem (Feng et al., 2013). However, the NTSMC system in (7) not only requires the nominal system dynamic but also results in the chattering phenomena. Thus, it is not suitable for real control applications.

3. Design of the INTSMC system

The proposed INTSMC system as shown in Fig. 1 is designed as

$$u_{ic} = u_{tc} + u_{rc} = -\hat{z}_o - \sum_{i=1}^{n-1} \lambda_i \frac{q_i}{p_i} \frac{d^{n-i} s_{i-2}}{dt^{n-i}}^{2-\frac{p_i}{q_i}} + u_{rc} \tag{11}$$

where the terminal neural controller u_{tc} serves as the main control, the output of PFNN $\hat{z}_o$ is utilized to online approximate the nonlinear term $z(\mathbf{x})$ in (3), and the robust compensator u_{rc} is designed to eliminate the effect of the approximation error upon system stability. The proposed ITSMC system needs only one neural approximator to online estimate the nonlinear

term. Thus, the proposed INTSMC system admits less computation complexity compared with traditional indirect INTSMC system.

3.1. Description of PFNN

There are m fuzzy rules in PFNN, which has n external inputs and one output as shown in Fig. 2. The *k*-th rule can be described as

$$\text{Rule } k\text{: IF } s_0 \text{ is } A_0^k \text{ and } \ldots \text{ and } s_{n-1} \text{ is } A_{n-1}^k, \text{ THEN } z_o \text{ is } \alpha_k \tag{12}$$

where A^k is the fuzzy set and α_k is the singleton. The operation functions of the nodes in each layer are introduced in the following.

Layer 1 (Input Layer): The input vector of is given by $[s_0, s_1, ..., s_{n-1}]^T = [u_1, ..., u_n]^T$, where u_i represents the *i*-th input to the node of layer 1.

Layer 2 (Membership Layer): Each function is described by a perturbed asymmetric membership function as follow (Karakose, 2010)

$$\mu_{ij} = \begin{cases} \exp\left(-\dfrac{(u_i - c_{ij})^2}{(\sigma_{ij}^L)^2}\right) - h_{ij}\sin(\omega_{ij}(u_i - c_{ij}))\cos(\omega_{ij}(u_i - c_{ij})), \text{ for } u_i < c_{ij} \\ \exp\left(-\dfrac{(u_i - c_{ij})^2}{(\sigma_{ij}^R)^2}\right) + h_{ij}\sin(\omega_{ij}(u_i - c_{ij}))\cos(\omega_{ij}(u_i - c_{ij})), \text{ for } u_i \geq c_{ij} \end{cases} \tag{13}$$

$$\varphi_{ij} = \begin{cases} 0 & \text{for } \mu_{ij} \leq 0 \\ 1 & \text{, for } \mu_{ij} \geq 1 \\ \mu_{ij} & \text{otherwise} \end{cases}, \text{ for } \quad j = 1, 2, \cdots, m \tag{14}$$

where μ_{ij} including adjustable parameters c_{ij}, σ_{ij}^L, σ_{ij}^R, ω_{ij} and h_{ij} presents the membership function. In (13), the first term denotes the asymmetric membership function with left-sided deviation (σ_{ij}^L) and right-sided deviation (σ_{ij}^R) to upgrade the learning capability, and the second term denotes the perturbation with adjustable frequency (ω_{ij}) and magnitude (h_{ij}) to handle information uncertainties. Figure 3 shows several perturbed

asymmetric membership functions with different frequencies and magnitudes. It can be seen that the special case of the perturbed asymmetric membership function when $h_{ij} = \omega_{ij} = 0$ is as the same as the asymmetric membership function in (Cheng et al., 2007; Lin et al., 2014). Further, the perturbed asymmetric membership function with a large frequency and magnitude acts likes the membership function of a type-2 fuzzy system in (Mendel, 2001).

Layer 3 (Rule Layer): The firing strength of the *k*-th rule is

$$\Theta_k = \prod_{i=1}^{n} \varphi_{ik} \text{ , for } k = 1,2,...,m \tag{15}$$

Layer 4 (Output Layer): The output of PFNN is obtained as

$$z_o = \sum_{k=1}^{m} \alpha_k \Theta_k \tag{16}$$

For ease of notation, the network output can be represented in a vector form as

$$z_o = \boldsymbol{\alpha}^T \boldsymbol{\Theta}(\mathbf{c}, \boldsymbol{\sigma}_\mathbf{L}, \boldsymbol{\sigma}_\mathbf{R}, \boldsymbol{\omega}, \mathbf{h}) = \boldsymbol{\alpha}^T \boldsymbol{\Theta} \tag{17}$$

where $\boldsymbol{\alpha} = [\alpha_1,..., \alpha_m]^T$, $\boldsymbol{\Theta} = [\Theta_1,..., \Theta_m]^T$, $\mathbf{c} = [c_{11},., c_{n1},..., c_{1m},., c_{nm}]^T$, $\boldsymbol{\sigma}_\mathbf{l} = [\sigma^L_{11},., \sigma^L_{n1},..., \sigma^L_{1m},., \sigma^L_{nm}]^T$, $\boldsymbol{\sigma}_\mathbf{r} = [\sigma^R_{11},., \sigma^R_{n1},..., \sigma^R_{1m},., \sigma^R_{nm}]^T$, $\boldsymbol{\omega} = [\omega_{11},., \omega_{n1},..., \omega_{1m},., \omega_{nm}]^T$ and $\mathbf{h} = [h_{11},., h_{n1},..., h_{1m},., h_{nm}]^T$. The output z_o of PFNN can be obtained directly without using the Karnik-Mendel iterative procedure. Thus, the computation cost of PFNN can be reduced. This leads the PFNN to be more practical.

According to the powerful approximation ability (Wang, 1994), it implies that there is an ideal PFNN which can uniformly approximate the nonlinear term $z(\mathbf{x})$ such as

$$z(\mathbf{x}) = \boldsymbol{\alpha}^{*T} \boldsymbol{\Theta}(\mathbf{c}^*, \boldsymbol{\sigma}^*_\mathbf{l}, \boldsymbol{\sigma}^*_\mathbf{r}, \boldsymbol{\omega}^*, \mathbf{h}^*) + \Delta = \boldsymbol{\alpha}^{*T} \boldsymbol{\Theta}^* + \Delta \tag{18}$$

where Δ is the approximation error, $\boldsymbol{\alpha}^*$, $\boldsymbol{\Theta}^*$, $\mathbf{c}^*$, $\boldsymbol{\sigma}^*_\mathbf{l}$, $\boldsymbol{\sigma}^*_\mathbf{r}$, $\boldsymbol{\omega}^*$ and $\mathbf{h}^*$ are the optimal vectors of $\boldsymbol{\alpha}$, $\boldsymbol{\Theta}$, $\mathbf{c}$, $\boldsymbol{\sigma}_\mathbf{l}$, $\boldsymbol{\sigma}_\mathbf{r}$, $\boldsymbol{\omega}$ and $\mathbf{h}$, respectively. In fact, the optimal vectors are difficult to determine. In the INTSMC scheme, an estimated PFNN is assumed to take the

following form

$$\hat{z}_o = \hat{\boldsymbol{\alpha}}^T \boldsymbol{\Theta}(\hat{\mathbf{c}}, \hat{\boldsymbol{\sigma}}_\mathbf{l}, \hat{\boldsymbol{\sigma}}_\mathbf{r}, \hat{\boldsymbol{\omega}}, \hat{\mathbf{h}}) = \hat{\boldsymbol{\alpha}}^T \hat{\boldsymbol{\Theta}} \tag{19}$$

where $\hat{\boldsymbol{\alpha}}$, $\hat{\boldsymbol{\Theta}}$, $\hat{\mathbf{c}}$, $\hat{\boldsymbol{\sigma}}_\mathbf{l}$, $\hat{\boldsymbol{\sigma}}_\mathbf{r}$, $\hat{\boldsymbol{\omega}}$ and $\hat{\mathbf{h}}$ are some estimates of the optimal vectors $\boldsymbol{\alpha}^*$, $\boldsymbol{\Theta}^*$, $\mathbf{c}^*$, $\boldsymbol{\sigma}_\mathbf{l}^*$, $\boldsymbol{\sigma}_\mathbf{r}^*$, $\boldsymbol{\omega}^*$ and $\mathbf{h}^*$, respectively. Subtracting (19) from (18), the estimation error can be obtained as

$$\begin{aligned} \tilde{z} &= z(\mathbf{x}) - \hat{z}_o \\ &= \tilde{\boldsymbol{\alpha}}^T \hat{\boldsymbol{\Theta}} + \hat{\boldsymbol{\alpha}}^T \tilde{\boldsymbol{\Theta}} + \tilde{\boldsymbol{\alpha}}^T \tilde{\boldsymbol{\Theta}} + \Delta \end{aligned} \tag{20}$$

where $\tilde{\boldsymbol{\alpha}} = \boldsymbol{\alpha}^* - \hat{\boldsymbol{\alpha}}$ and $\tilde{\boldsymbol{\Theta}} = \boldsymbol{\Theta}^* - \hat{\boldsymbol{\Theta}}$. The linearization technique is employed to transform the perturbed asymmetric membership functions into partially linear form by the usage of Taylor series expansion, where $\tilde{\boldsymbol{\Theta}}$ can be obtained as (Hsu and Kuo, 2014)

$$\tilde{\boldsymbol{\Theta}} = \mathbf{A}^T \tilde{\mathbf{c}} + \mathbf{B}_\mathbf{l}^T \tilde{\boldsymbol{\sigma}}_\mathbf{l} + \mathbf{B}_\mathbf{r}^T \tilde{\boldsymbol{\sigma}}_\mathbf{r} + \mathbf{C}^T \tilde{\boldsymbol{\omega}} + \mathbf{D}^T \tilde{\mathbf{h}} + \mathbf{o} \tag{21}$$

where $\tilde{\mathbf{c}} = \mathbf{c}^* - \hat{\mathbf{c}}$, $\tilde{\boldsymbol{\sigma}}_\mathbf{l} = \boldsymbol{\sigma}_\mathbf{l}^* - \hat{\boldsymbol{\sigma}}_\mathbf{l}$, $\tilde{\boldsymbol{\sigma}}_\mathbf{r} = \boldsymbol{\sigma}_\mathbf{r}^* - \hat{\boldsymbol{\sigma}}_\mathbf{r}$, $\tilde{\boldsymbol{\omega}} = \boldsymbol{\omega}^* - \hat{\boldsymbol{\omega}}$, $\tilde{\mathbf{h}} = \mathbf{h}^* - \hat{\mathbf{h}}$, $\mathbf{o}$ is a vector of high order terms, $\mathbf{A} = \left[\frac{\partial \Theta_1}{\partial \mathbf{c}} \cdots \frac{\partial \Theta_m}{\partial \mathbf{c}} \right]|_{\mathbf{c}=\hat{\mathbf{c}}}$, $\mathbf{B}_\mathbf{l} = \left[\frac{\partial \Theta_1}{\partial \boldsymbol{\sigma}_\mathbf{l}} \cdots \frac{\partial \Theta_m}{\partial \boldsymbol{\sigma}_\mathbf{l}} \right]|_{\boldsymbol{\sigma}_\mathbf{l}=\hat{\boldsymbol{\sigma}}_\mathbf{l}}$, $\mathbf{B}_\mathbf{r} = \left[\frac{\partial \Theta_1}{\partial \boldsymbol{\sigma}_\mathbf{r}} \cdots \frac{\partial \Theta_m}{\partial \boldsymbol{\sigma}_\mathbf{r}} \right]|_{\boldsymbol{\sigma}_\mathbf{r}=\hat{\boldsymbol{\sigma}}_\mathbf{r}}$, $\mathbf{C} = \left[\frac{\partial \Theta_1}{\partial \boldsymbol{\omega}} \cdots \frac{\partial \Theta_m}{\partial \boldsymbol{\omega}} \right]|_{\boldsymbol{\omega}=\hat{\boldsymbol{\omega}}}$ and $\mathbf{D} = \left[\frac{\partial \Theta_1}{\partial \mathbf{h}} \cdots \frac{\partial \Theta_m}{\partial \mathbf{h}} \right]|_{\mathbf{h}=\hat{\mathbf{h}}}$. Substituting (21) into (20) yields

$$\begin{aligned} \tilde{z} &= \tilde{\boldsymbol{\alpha}}^T \hat{\boldsymbol{\Theta}} + \hat{\boldsymbol{\alpha}}^T (\mathbf{A}^T \tilde{\mathbf{c}} + \mathbf{B}_\mathbf{l}^T \tilde{\boldsymbol{\sigma}}_\mathbf{l} + \mathbf{B}_\mathbf{r}^T \tilde{\boldsymbol{\sigma}}_\mathbf{r} + \mathbf{C}^T \tilde{\boldsymbol{\omega}} + \mathbf{D}^T \tilde{\mathbf{h}} + \mathbf{o}) + \tilde{\boldsymbol{\alpha}}^T \tilde{\boldsymbol{\Theta}} + \Delta \\ &= \tilde{\boldsymbol{\alpha}}^T \hat{\boldsymbol{\Theta}} + \tilde{\mathbf{c}}^T \mathbf{A} \hat{\boldsymbol{\alpha}} + \tilde{\boldsymbol{\sigma}}_\mathbf{l}^T \mathbf{B}_\mathbf{l} \hat{\boldsymbol{\alpha}} + \tilde{\boldsymbol{\sigma}}_\mathbf{r}^T \mathbf{B}_\mathbf{r} \hat{\boldsymbol{\alpha}} + \tilde{\boldsymbol{\omega}}^T \mathbf{C} \hat{\boldsymbol{\alpha}} + \tilde{\mathbf{h}}^T \mathbf{D} \hat{\boldsymbol{\alpha}} + \varepsilon \end{aligned} \tag{22}$$

where $\varepsilon = \hat{\boldsymbol{\alpha}}^T \mathbf{o} + \tilde{\boldsymbol{\alpha}}^T \tilde{\boldsymbol{\Theta}} + \Delta$ denotes a lump approximation error, $\hat{\boldsymbol{\alpha}}^T \mathbf{A}^T \tilde{\mathbf{c}} = \tilde{\mathbf{c}}^T \mathbf{A} \hat{\boldsymbol{\alpha}}$, $\hat{\boldsymbol{\alpha}}^T \mathbf{B}_\mathbf{l}^T \tilde{\boldsymbol{\sigma}}_\mathbf{l} = \tilde{\boldsymbol{\sigma}}_\mathbf{l}^T \mathbf{B}_\mathbf{l} \hat{\boldsymbol{\alpha}}$, $\hat{\boldsymbol{\alpha}}^T \mathbf{B}_\mathbf{r}^T \tilde{\boldsymbol{\sigma}}_\mathbf{r} = \tilde{\boldsymbol{\sigma}}_\mathbf{r}^T \mathbf{B}_\mathbf{r} \hat{\boldsymbol{\alpha}}$, $\hat{\boldsymbol{\alpha}}^T \mathbf{C}^T \tilde{\boldsymbol{\omega}} = \tilde{\boldsymbol{\omega}}^T \mathbf{C} \hat{\boldsymbol{\alpha}}$ and $\hat{\boldsymbol{\alpha}}^T \mathbf{D}^T \tilde{\mathbf{h}} = \tilde{\mathbf{h}}^T \mathbf{D} \hat{\boldsymbol{\alpha}}$. The lump approximation error ε can be bounded by $0 \le |\varepsilon| \le E$ where E is a positive constant (Lin and Li, 2012).

3.2. Parameter learning

Differentiating (5) with respect to time and imposing the control law $u = u_{ic}$ into (3) yields

$$\begin{aligned}\dot{s}_{n-1} &= \dot{s}_{n-2} + \frac{1}{\lambda_{n-1}}\frac{p_{n-1}}{q_{n-1}}\dot{s}_{n-2}^{\frac{p_{n-1}}{q_{n-1}}-1}\dot{s}_{n-2} \\ &= \frac{1}{\lambda_{n-1}}\frac{p_{n-1}}{q_{n-1}}\dot{s}_{n-2}^{\frac{p_{n-1}}{q_{n-1}}-1}[z(\mathbf{x}) - \hat{z}_o + u_{rc}] \\ &= \delta_{n-2}[z(\mathbf{x}) - \hat{z}_o + u_{rc}] \end{aligned} \tag{23}$$

where $\delta_{n-2} = \frac{1}{\lambda_{n-1}}\frac{p_{n-1}}{q_{n-1}}\dot{s}_{n-2}^{\frac{p_{n-1}}{q_{n-1}}-1}$. Substituting (22) into (23) yields

$$\dot{s}_{n-1} = \delta_{n-2}(\tilde{\boldsymbol{\alpha}}^T\hat{\boldsymbol{\Theta}} + \tilde{\mathbf{c}}^T\mathbf{A}\hat{\boldsymbol{\alpha}} + \tilde{\boldsymbol{\sigma}}_{\mathbf{l}}^T\mathbf{B}_{\mathbf{l}}\hat{\boldsymbol{\alpha}} + \tilde{\boldsymbol{\sigma}}_{\mathbf{r}}^T\mathbf{B}_{\mathbf{r}}\hat{\boldsymbol{\alpha}} + \tilde{\boldsymbol{\omega}}^T\mathbf{C}\hat{\boldsymbol{\alpha}} + \tilde{\mathbf{h}}^T\mathbf{D}\hat{\boldsymbol{\alpha}} + \varepsilon + u_{rc}) \tag{24}$$

In this study, the robust compensator u_{rc} is designed as

$$u_{rc} = -Ks_{n-1} - \frac{E}{\rho + (1-\rho)e^{-\gamma|s_{n-1}|}}\tanh(\frac{s_{n-1}}{\Phi}) \tag{25}$$

where K is a positive constant, $\tanh(\cdot)$ is the hyperbolic tangent function, ρ is a strictly positive constant that is less than one, γ is a strictly positive integer and Φ is the bound layer of the sliding surface s_{n-1}. It can be seen that the term $\frac{E}{\rho + (1-\rho)e^{-\gamma|s_{n-1}|}}$ dynamically varies between E and $\frac{E}{\rho}$ by the variations of the $|s_{n-1}|$. If $|s_{n-1}|$ increases, the term $\frac{E}{\rho + (1-\rho)e^{-\gamma|s_{n-1}|}}$ converges to $\frac{E}{\rho}$ which is greater than E. It implies that the robust compensator can dynamically increases the control gain to obtain a faster reaching time, a good robustness and tracking performance.

To guarantee the stability of the proposed INTSMC system, consider a Lyapunov function candidate in the following form as

$$V(t)=\frac{1}{2}s_{n-1}{}^{2}+\frac{\tilde{\boldsymbol{\alpha}}^{T}\tilde{\boldsymbol{\alpha}}}{2\eta_{\alpha}}+\frac{\tilde{\mathbf{c}}^{T}\tilde{\mathbf{c}}}{2\eta_{c}}+\frac{\tilde{\boldsymbol{\sigma}}_{\mathbf{l}}^{T}\tilde{\boldsymbol{\sigma}}_{\mathbf{l}}}{2\eta_{l}}+\frac{\tilde{\boldsymbol{\sigma}}_{\mathbf{r}}^{T}\tilde{\boldsymbol{\sigma}}_{\mathbf{r}}}{2\eta_{r}}+\frac{\tilde{\boldsymbol{\omega}}^{T}\tilde{\boldsymbol{\omega}}}{2\eta_{\omega}}+\frac{\tilde{\mathbf{h}}^{T}\tilde{\mathbf{h}}}{2\eta_{h}} \tag{26}$$

where η_{α}, η_{c}, η_{l}, η_{r}, η_{ω} and η_{h} are positive learning constants. Differentiating (26) with respect to time and using (24) and (25), we have

$$\begin{aligned}\dot{V}(t)&=s_{n-1}\dot{s}_{n-1}+\frac{\tilde{\boldsymbol{\alpha}}^{T}\dot{\tilde{\boldsymbol{\alpha}}}}{\eta_{\alpha}}+\frac{\tilde{\mathbf{c}}^{T}\dot{\tilde{\mathbf{c}}}}{\eta_{c}}+\frac{\tilde{\boldsymbol{\sigma}}_{\mathbf{l}}^{T}\dot{\tilde{\boldsymbol{\sigma}}}_{\mathbf{l}}}{\eta_{l}}+\frac{\tilde{\boldsymbol{\sigma}}_{\mathbf{r}}^{T}\dot{\tilde{\boldsymbol{\sigma}}}_{\mathbf{r}}}{\eta_{r}}+\frac{\tilde{\boldsymbol{\omega}}^{T}\dot{\tilde{\boldsymbol{\omega}}}}{\eta_{\omega}}+\frac{\tilde{\mathbf{h}}^{T}\dot{\tilde{\mathbf{h}}}}{\eta_{h}}\\&=s_{n-1}\delta_{n-2}(\tilde{\boldsymbol{\alpha}}^{T}\hat{\boldsymbol{\Theta}}+\tilde{\mathbf{c}}^{T}\mathbf{A}\hat{\boldsymbol{\alpha}}+\tilde{\boldsymbol{\sigma}}_{\mathbf{l}}^{T}\mathbf{B}_{\mathbf{l}}\hat{\boldsymbol{\alpha}}+\tilde{\boldsymbol{\sigma}}_{\mathbf{r}}^{T}\mathbf{B}_{\mathbf{r}}\hat{\boldsymbol{\alpha}}+\tilde{\boldsymbol{\omega}}^{T}\mathbf{C}\hat{\boldsymbol{\alpha}}+\tilde{\mathbf{h}}^{T}\mathbf{D}\hat{\boldsymbol{\alpha}}+\varepsilon+u_{rc})\\&\quad+\frac{\tilde{\boldsymbol{\alpha}}^{T}\dot{\tilde{\boldsymbol{\alpha}}}}{\eta_{\alpha}}+\frac{\tilde{\mathbf{c}}^{T}\dot{\tilde{\mathbf{c}}}}{\eta_{c}}+\frac{\tilde{\boldsymbol{\sigma}}_{\mathbf{l}}^{T}\dot{\tilde{\boldsymbol{\sigma}}}_{\mathbf{l}}}{\eta_{l}}+\frac{\tilde{\boldsymbol{\sigma}}_{\mathbf{r}}^{T}\dot{\tilde{\boldsymbol{\sigma}}}_{\mathbf{r}}}{\eta_{r}}+\frac{\tilde{\boldsymbol{\omega}}^{T}\dot{\tilde{\boldsymbol{\omega}}}}{\eta_{\omega}}+\frac{\tilde{\mathbf{h}}^{T}\dot{\tilde{\mathbf{h}}}}{\eta_{h}}\\&=\tilde{\boldsymbol{\alpha}}^{T}(\delta_{n-2}s_{n-1}\hat{\boldsymbol{\Theta}}+\frac{\dot{\tilde{\boldsymbol{\alpha}}}}{\eta_{\alpha}})+\tilde{\mathbf{c}}^{T}(\delta_{n-2}s_{n-1}\mathbf{A}\hat{\boldsymbol{\alpha}}+\frac{\dot{\tilde{\mathbf{c}}}}{\eta_{c}})+\tilde{\boldsymbol{\sigma}}_{\mathbf{l}}^{T}(\delta_{n-2}s_{n-1}\mathbf{B}_{\mathbf{l}}\hat{\boldsymbol{\alpha}}+\frac{\dot{\tilde{\boldsymbol{\sigma}}}_{\mathbf{l}}}{\eta_{l}})\\&\quad+\tilde{\boldsymbol{\sigma}}_{\mathbf{r}}^{T}(\delta_{n-2}s_{n-1}\mathbf{B}_{\mathbf{r}}\hat{\boldsymbol{\alpha}}+\frac{\dot{\tilde{\boldsymbol{\sigma}}}_{\mathbf{r}}}{\eta_{r}})+\tilde{\boldsymbol{\omega}}^{T}(\delta_{n-2}s_{n-1}\mathbf{C}\hat{\boldsymbol{\alpha}}+\frac{\dot{\tilde{\boldsymbol{\omega}}}}{\eta_{\omega}})+\tilde{\mathbf{h}}^{T}(\delta_{n-2}s_{n-1}\mathbf{D}\hat{\boldsymbol{\alpha}}+\frac{\dot{\tilde{\mathbf{h}}}}{\eta_{h}})\\&\quad+s_{n-1}\delta_{n-2}(\varepsilon+u_{rc})\end{aligned} \tag{27}$$

Choose the parameter adaptation laws as

$$\dot{\hat{\boldsymbol{\alpha}}}=-\dot{\tilde{\boldsymbol{\alpha}}}=\eta_{\alpha}[\delta_{n-2}s_{n-1}\hat{\boldsymbol{\Theta}}-\mu_{\alpha}(\hat{\boldsymbol{\alpha}}-\bar{\boldsymbol{\alpha}})] \tag{28}$$

$$\dot{\hat{\mathbf{c}}}=-\dot{\tilde{\mathbf{c}}}=\eta_{c}[\delta_{n-2}s_{n-1}\mathbf{A}\hat{\boldsymbol{\alpha}}-\mu_{c}(\hat{\mathbf{c}}-\bar{\mathbf{c}})] \tag{29}$$

$$\dot{\hat{\boldsymbol{\sigma}}}_{\mathbf{l}}=-\dot{\tilde{\boldsymbol{\sigma}}}_{\mathbf{l}}=\eta_{l}[\delta_{n-2}s_{n-1}\mathbf{B}_{\mathbf{l}}\hat{\boldsymbol{\alpha}}-\mu_{l}(\hat{\boldsymbol{\sigma}}_{\mathbf{l}}-\bar{\boldsymbol{\sigma}}_{\mathbf{l}})] \tag{30}$$

$$\dot{\hat{\boldsymbol{\sigma}}}_{\mathbf{r}}=-\dot{\tilde{\boldsymbol{\sigma}}}_{\mathbf{r}}=\eta_{r}[\delta_{n-2}s_{n-1}\mathbf{B}_{\mathbf{r}}\hat{\boldsymbol{\alpha}}-\mu_{r}(\hat{\boldsymbol{\sigma}}_{\mathbf{r}}-\bar{\boldsymbol{\sigma}}_{\mathbf{r}})] \tag{31}$$

$$\dot{\hat{\boldsymbol{\omega}}}=-\dot{\tilde{\boldsymbol{\omega}}}=\eta_{\omega}[\delta_{n-2}s_{n-1}\mathbf{C}\hat{\boldsymbol{\alpha}}-\mu_{\omega}(\hat{\boldsymbol{\omega}}-\bar{\boldsymbol{\omega}})] \tag{32}$$

$$\dot{\hat{\mathbf{h}}}=-\dot{\tilde{\mathbf{h}}}=\eta_{h}[\delta_{n-2}s_{n-1}\mathbf{D}\hat{\boldsymbol{\alpha}}-\mu_{h}(\hat{\mathbf{h}}-\bar{\mathbf{h}})] \tag{33}$$

where μ_{α}, μ_{c}, μ_{l}, μ_{r}, μ_{ω} and μ_{h} are small positive constants, and $\bar{\boldsymbol{\alpha}}$, $\bar{\mathbf{c}}$, $\bar{\boldsymbol{\sigma}}_{\mathbf{l}}$, $\bar{\boldsymbol{\sigma}}_{\mathbf{r}}$, $\bar{\boldsymbol{\omega}}$ and $\bar{\mathbf{h}}$ are the initial parameter vectors of $\hat{\boldsymbol{\alpha}}$, $\hat{\mathbf{c}}$, $\hat{\boldsymbol{\sigma}}_{\mathbf{l}}$, $\hat{\boldsymbol{\sigma}}_{\mathbf{r}}$, $\hat{\boldsymbol{\omega}}$ and $\hat{\mathbf{h}}$, respectively, then (27) becomes

$$\dot{V}(t) = \mu_\alpha \tilde{\boldsymbol{\alpha}}^T(\hat{\boldsymbol{\alpha}} - \overline{\boldsymbol{\alpha}}) + \mu_c \tilde{\mathbf{c}}^T(\hat{\mathbf{c}} - \overline{\mathbf{c}}) + \mu_l \tilde{\boldsymbol{\sigma}}_\mathbf{l}^T(\hat{\boldsymbol{\sigma}}_\mathbf{l} - \overline{\boldsymbol{\sigma}}_\mathbf{l}) + \mu_r \tilde{\boldsymbol{\sigma}}_\mathbf{r}^T(\hat{\boldsymbol{\sigma}}_\mathbf{r} - \overline{\boldsymbol{\sigma}}_\mathbf{r})$$
$$+ \mu_\omega \tilde{\boldsymbol{\omega}}^T(\hat{\boldsymbol{\omega}} - \overline{\boldsymbol{\omega}}) + \mu_h \tilde{\mathbf{h}}^T(\hat{\mathbf{h}} - \overline{\mathbf{h}}) + \varepsilon \delta_{n-2} s_{n-1}$$
$$- K\delta_{n-2} {s_{n-1}}^2 - \frac{E}{\rho + (1-\rho)e^{-\gamma|s_{n-1}|}} \delta_{n-2} s_{n-1} \tanh(\frac{s_{n-1}}{\Phi})$$
$$\le \mu_\alpha \tilde{\boldsymbol{\alpha}}^T(\hat{\boldsymbol{\alpha}} - \overline{\boldsymbol{\alpha}}) + \mu_c \tilde{\mathbf{c}}^T(\hat{\mathbf{c}} - \overline{\mathbf{c}}) + \mu_l \tilde{\boldsymbol{\sigma}}_\mathbf{l}^T(\hat{\boldsymbol{\sigma}}_\mathbf{l} - \overline{\boldsymbol{\sigma}}_\mathbf{l}) + \mu_r \tilde{\boldsymbol{\sigma}}_\mathbf{r}^T(\hat{\boldsymbol{\sigma}}_\mathbf{r} - \overline{\boldsymbol{\sigma}}_\mathbf{r})$$
$$+ \mu_\omega \tilde{\boldsymbol{\omega}}^T(\hat{\boldsymbol{\omega}} - \overline{\boldsymbol{\omega}}) + \mu_h \tilde{\mathbf{h}}^T(\hat{\mathbf{h}} - \overline{\mathbf{h}}) + |\varepsilon| \delta_{n-2} |s_{n-1}|$$
$$- K\delta_{n-2} {s_{n-1}}^2 - E\delta_{n-2} s_{n-1} \tanh(\frac{s_{n-1}}{\Phi})$$
$$\le \mu_\alpha \tilde{\boldsymbol{\alpha}}^T(\hat{\boldsymbol{\alpha}} - \overline{\boldsymbol{\alpha}}) + \mu_c \tilde{\mathbf{c}}^T(\hat{\mathbf{c}} - \overline{\mathbf{c}}) + \mu_l \tilde{\boldsymbol{\sigma}}_\mathbf{l}^T(\hat{\boldsymbol{\sigma}}_\mathbf{l} - \overline{\boldsymbol{\sigma}}_\mathbf{l}) + \mu_r \tilde{\boldsymbol{\sigma}}_\mathbf{r}^T(\hat{\boldsymbol{\sigma}}_\mathbf{r} - \overline{\boldsymbol{\sigma}}_\mathbf{r})$$
$$+ \mu_\omega \tilde{\boldsymbol{\omega}}^T(\hat{\boldsymbol{\omega}} - \overline{\boldsymbol{\omega}}) + \mu_h \tilde{\mathbf{h}}^T(\hat{\mathbf{h}} - \overline{\mathbf{h}}) - K\delta_{n-2} {s_{n-1}}^2$$
$$+ E\delta_{n-2}[|s_{n-1}| - s_{n-1} \tanh(\frac{s_{n-1}}{\Phi})] \tag{34}$$

It can be found that the following inequality holds for any $\Phi > 0$ as (Kim and Calise, 2007)

$$0 \le |s_{n-1}| - s_{n-1} \tanh(\frac{s_{n-1}}{\Phi}) \le \beta\Phi \tag{35}$$

where β is a constant satisfying $\beta = e^{-(\beta+1)}$. Using the inequality (35), (34) can be rewritten as

$$\dot{V}(t) \le \mu_\alpha \tilde{\boldsymbol{\alpha}}^T(\hat{\boldsymbol{\alpha}} - \overline{\boldsymbol{\alpha}}) + \mu_c \tilde{\mathbf{c}}^T(\hat{\mathbf{c}} - \overline{\mathbf{c}}) + \mu_l \tilde{\boldsymbol{\sigma}}_\mathbf{l}^T(\hat{\boldsymbol{\sigma}}_\mathbf{l} - \overline{\boldsymbol{\sigma}}_\mathbf{l}) + \mu_r \tilde{\boldsymbol{\sigma}}_\mathbf{r}^T(\hat{\boldsymbol{\sigma}}_\mathbf{r} - \overline{\boldsymbol{\sigma}}_\mathbf{r})$$
$$+ \mu_\omega \tilde{\boldsymbol{\omega}}^T(\hat{\boldsymbol{\omega}} - \overline{\boldsymbol{\omega}}) + \mu_h \tilde{\mathbf{h}}^T(\hat{\mathbf{h}} - \overline{\mathbf{h}}) - K\delta_{n-2} {s_{n-1}}^2 + E\delta_{n-2}\beta\Phi$$
$$= \mu_\alpha(\boldsymbol{\alpha}^* - \hat{\boldsymbol{\alpha}})^T(\hat{\boldsymbol{\alpha}} - \overline{\boldsymbol{\alpha}}) + \mu_c(\mathbf{c}^* - \hat{\mathbf{c}})^T(\hat{\mathbf{c}} - \overline{\mathbf{c}}) + \mu_l(\boldsymbol{\sigma}_\mathbf{l}^* - \hat{\boldsymbol{\sigma}}_\mathbf{l})(\hat{\boldsymbol{\sigma}}_\mathbf{l} - \overline{\boldsymbol{\sigma}}_\mathbf{l})$$
$$+ \mu_r(\boldsymbol{\sigma}_\mathbf{r}^* - \hat{\boldsymbol{\sigma}}_\mathbf{r})(\hat{\boldsymbol{\sigma}}_\mathbf{r} - \overline{\boldsymbol{\sigma}}_\mathbf{r}) + \mu_\omega(\boldsymbol{\omega}^* - \hat{\boldsymbol{\omega}})(\hat{\boldsymbol{\omega}} - \overline{\boldsymbol{\omega}}) + \mu_h(\mathbf{h}^* - \hat{\mathbf{h}})(\hat{\mathbf{h}} - \overline{\mathbf{h}})$$
$$- K\delta_{n-2} {s_{n-1}}^2 + E\delta_{n-2}\beta\Phi$$
$$\le -\frac{\mu_\alpha}{2}(\|\boldsymbol{\alpha}^* - \hat{\boldsymbol{\alpha}}\|^2 - \|\boldsymbol{\alpha}^* - \overline{\boldsymbol{\alpha}}\|^2 + \|\hat{\boldsymbol{\alpha}} - \overline{\boldsymbol{\alpha}}\|^2)$$

$$-\frac{\mu_c}{2}(\left\|\mathbf{c}^*-\hat{\mathbf{c}}\right\|^2-\left\|\mathbf{c}^*-\bar{\mathbf{c}}\right\|^2+\left\|\hat{\mathbf{c}}-\bar{\mathbf{c}}\right\|^2)$$

$$-\frac{\mu_l}{2}(\left\|\boldsymbol{\sigma}_\mathbf{l}^*-\hat{\boldsymbol{\sigma}}_\mathbf{l}\right\|^2-\left\|\boldsymbol{\sigma}_\mathbf{l}^*-\bar{\boldsymbol{\sigma}}_\mathbf{l}\right\|^2+\left\|\hat{\boldsymbol{\sigma}}_\mathbf{l}-\bar{\boldsymbol{\sigma}}_\mathbf{l}\right\|^2)$$

$$-\frac{\mu_r}{2}(\left\|\boldsymbol{\sigma}_\mathbf{r}^*-\hat{\boldsymbol{\sigma}}_\mathbf{r}\right\|^2-\left\|\boldsymbol{\sigma}_\mathbf{r}^*-\bar{\boldsymbol{\sigma}}_\mathbf{r}\right\|^2+\left\|\hat{\boldsymbol{\sigma}}_\mathbf{r}-\bar{\boldsymbol{\sigma}}_\mathbf{r}\right\|^2)$$

$$-\frac{\mu_\omega}{2}(\left\|\boldsymbol{\omega}^*-\hat{\boldsymbol{\omega}}\right\|^2-\left\|\boldsymbol{\omega}^*-\bar{\boldsymbol{\omega}}\right\|^2+\left\|\hat{\boldsymbol{\omega}}-\bar{\boldsymbol{\omega}}\right\|^2)$$

$$-\frac{\mu_h}{2}(\left\|\mathbf{h}^*-\hat{\mathbf{h}}\right\|^2-\left\|\mathbf{h}^*-\bar{\mathbf{h}}\right\|^2+\left\|\hat{\mathbf{h}}-\bar{\mathbf{h}}\right\|^2)$$

$$-K\delta_{n-2}{s_{n-1}}^2+E\delta_{n-2}\beta\Phi$$

$$\leq -K\delta_{n-2}{s_{n-1}}^2-\frac{\mu_\alpha}{2}\left\|\tilde{\boldsymbol{\alpha}}\right\|^2-\frac{\mu_c}{2}\left\|\tilde{\mathbf{c}}\right\|^2-\frac{\mu_l}{2}\left\|\tilde{\boldsymbol{\sigma}}_\mathbf{l}\right\|^2-\frac{\mu_r}{2}\left\|\tilde{\boldsymbol{\sigma}}_r\right\|^2-\frac{\mu_\omega}{2}\left\|\tilde{\boldsymbol{\omega}}\right\|^2-\frac{\mu_h}{2}\left\|\tilde{\mathbf{h}}\right\|^2$$

$$+\frac{\mu_\alpha}{2}\left\|\boldsymbol{\alpha}^*-\bar{\boldsymbol{\alpha}}\right\|^2+\frac{\mu_c}{2}\left\|\mathbf{c}^*-\bar{\mathbf{c}}\right\|^2+\frac{\mu_l}{2}\left\|\boldsymbol{\sigma}_\mathbf{l}^*-\bar{\boldsymbol{\sigma}}_\mathbf{l}\right\|^2+\frac{\mu_r}{2}\left\|\boldsymbol{\sigma}_\mathbf{r}^*-\bar{\boldsymbol{\sigma}}_\mathbf{r}\right\|^2$$

$$+\frac{\mu_\omega}{2}\left\|\boldsymbol{\omega}^*-\bar{\boldsymbol{\omega}}\right\|^2+\frac{\mu_h}{2}\left\|\mathbf{h}^*-\bar{\mathbf{h}}\right\|^2+E\delta_{n-2}\beta\Phi \tag{36}$$

where $\|\cdot\|$ denotes an induced norm. Define c and d are positive constants given as

$$c=\min(K\delta_{n-2},\mu_\alpha\eta_\alpha,\mu_c\eta_c,\mu_l\eta_l,\mu_r\eta_r,\mu_\omega\eta_\omega,\mu_h\eta_h) \tag{37}$$

$$d=\frac{1}{2}(\mu_\alpha\left\|\boldsymbol{\alpha}^*-\bar{\boldsymbol{\alpha}}\right\|^2+\mu_c\left\|\mathbf{c}^*-\mathbf{c}_0\right\|^2+\mu_l\left\|\boldsymbol{\sigma}_\mathbf{l}^*-\bar{\boldsymbol{\sigma}}_\mathbf{l}\right\|^2+\mu_r\left\|\boldsymbol{\sigma}_\mathbf{r}^*-\bar{\boldsymbol{\sigma}}_\mathbf{r}\right\|^2)$$

$$+\mu_\omega\left\|\boldsymbol{\omega}^*-\bar{\boldsymbol{\omega}}\right\|^2+\mu_h\left\|\mathbf{h}^*-\bar{\mathbf{h}}\right\|^2)+E\delta_{n-2}\beta\Phi \tag{38}$$

thus (36) can be rewritten as

$$\dot{V}(t)\leq cV(t)+d \tag{39}$$

Since $\frac{d}{c}>0$ and the solution of the differential inequality (39) satisfies (Lin and Li, 2013)

$$0\leq V(t)\leq\frac{d}{c}+[V(0)-\frac{d}{c}]e^{-ct} \tag{40}$$

where $V(0)$ is the initial value of $V(t)$, then the estimated vectors $\hat{\boldsymbol{\alpha}}$, $\hat{\boldsymbol{\Theta}}$, $\hat{\mathbf{c}}$, $\hat{\boldsymbol{\sigma}}_{\mathbf{l}}$, $\hat{\boldsymbol{\sigma}}_{\mathbf{r}}$, $\hat{\boldsymbol{\omega}}$ and $\hat{\mathbf{h}}$ are uniformly ultimately bounded. From (40), it is obtained that

$$\frac{1}{2}s^2(t) \le \frac{d}{c} + V(0)e^{-ct} \tag{41}$$

which implies that, given $\rho > \sqrt{\frac{2d}{c}}$, the tracking index satisfies

$$s(t) < \rho \tag{42}$$

where ρ is the size of a small residual set that depends on the PFNN approximation error and the INTSMC controller parameters. It implies that the output of the INTSMC system can exponentially converge to a small neighborhood of the trajectory command (Kim and Calise, 2007; Lin and Li, 2013; Na et al., 2013).

Remark 1: Though the control chattering has been eliminated by using the smooth compensator in (Kim and Calise, 2007; Lin and Li, 2013; Na et al., 2013), the convergence speed of tacking error is slow due to the control gain of the smooth compensator is fixed. In the proposed control scheme, the control gain of the robust compensator in (25) dynamically increases to obtain a good robustness and to speed up the convergence speed of tacking error without chattering problem. Thus, the proposed robust compensator could be more suitable than the smooth compensator in (Kim and Calise, 2007; Lin and Li, 2013; Na et al., 2013).

4. Simulation and experimental results

It should be emphasized that the proposed INTSMC system requires no prior knowledge of the system dynamics. The parameters λ_i, p_i and q_i for the nonsingular terminal sliding surface offers some superior properties such as finite time convergence. Selections of the learning rates (η_α, μ_α, η_c, μ_c, η_l, μ_l, η_r, μ_r, η_ω, μ_ω, η_h and μ_h) for online training have a significant effect on the PFNN learning performance. If necessary, the

variable optimal learning rates can be derived using the algorithms presented in (Lin and Li, 2015) to speed up parameter learning. The constants K and E will influence the convergent speed of the tracking error and the constant ρ will attenuate a desired level of approximation error. It is known that the determining an appropriate number of fuzzy rules m in PFNN is an important issue because of the trade off between a computational loading and a learning performance. In general, if the number of fuzzy rules is large, the computational loading is heavy so that it is not suitable for online practical applications. If the number of fuzzy rules is small, the learning performance may be not good enough to achieve desired control performance. In this paper, the number of the used fuzzy rules is determined by some trial-and-error tuning procedures.

Example 1: inverted pendulum

Consider an inverted pendulum stabilizing problem, the dynamic equation of the inverted pendulum system is given as Wang (1994)

$$\ddot{x} = f(\mathbf{x}) + g(\mathbf{x})u \tag{43}$$

where x is the angle of the pendulum with respect to the vertical line, $\mathbf{x} = [x, \dot{x}]^T$ is the state vector, m_c is the mass of cart, m_r is the mass of rod, $\bar{g}$ is the acceleration due to gravity, l is the half length of rod, $f(\mathbf{x}) = \dfrac{m_r l \dot{x}^2 \sin(x)\cos(x) - (m_c + m_r)\bar{g}\sin(x)}{m_r l \cos^2(x) - \frac{4}{3} l (m_c + m_r)}$ and

$g(\mathbf{x}) = \dfrac{-\cos(x)}{m_r l \cos^2(x) - \frac{4}{3} l (m_c + m_r)}$ are the system dynamics, and u is the control input. In this example, it is assumed that $\bar{g} = 9.81$, $m_c = 1$, $m_r = 0.1$, and $l = 0.5$. To illustrate the effectiveness of the proposed INTSMC system, an external disturbance $d = 3\sin(4t)\cos(8t)$ is generated starting from $t = 20\,\text{sec}$. The parameters of the proposed INTSMC system are selected as $\lambda_1 = 0.5$, $p_1 = 7$, $q_1 = 5$, $\eta_\alpha = 20$, $\eta_c = \eta_l = \eta_r = \eta_\omega = \eta_h = 1$,

$\mu_\alpha = \mu_c = \mu_l = \mu_r = \mu_\omega = \mu_h = 0.001$, $K = 1$, $\rho = 0.5$, $\gamma = 1$, $E = 0.1$ and $\Phi = 0.05$. All of the parameters are determined by trial and error in order to guarantee the desired control performance.

For the comparison of the control performance, first, the simulation results of the dynamic fuzzy neural control (Lin and Li, 2015) are shown in Fig. 4. The simulation results show that the dynamic fuzzy neural control system can achieve favorable control performance. Due to the supervised gradient-descent method is used to develop the parameter learning law, the system stability has not been guaranteed so far.

Then, a type-1 fuzzy neural network (T1FNN) which can be found in (Lin et al., 2014) is used to approximate the nonlinear term of the system dynamics. The simulation results of the INTSMC system with T1FNN are shown in Fig. 5. The simulation results show that the INTSMC system with T1FNN can achieve favorable control performance and is robust against external disturbance after T1FNN learning. Meanwhile, an interval T2FNN which can be found in (Chang and Chan, 2014) is used to approximate the nonlinear term of the system dynamics again. The simulation results of the INTSMC system with T2FNN are shown in Fig. 6. The simulation results show that the INTSMC system with T2FNN can achieve more favorable tracking performance with faster convergence speed of the tracking error.

Finally, the proposed PFNN is used to approximate the nonlinear term of the system dynamics again. The simulation results of the INTSMC system with PFNN are shown in Fig. 7. The simulation results verify that the proposed INTSMC system with PFNN can achieve the favorable tracking performance even under an external disturbance occurs. Moreover, to demonstrate the robust tracking capability of the INTSMC system with PFNN, a payload is added to the inverted pendulum with $m_c = 2$. Tracking responses with payload are shown in Fig. 8. The simulation results show that favorable control performance can be achieved after controller parameters learning and is robust against parameter variations in the plant.

In summary, a performance comparison between the dynamic fuzzy neural control, the INTSMC with T1FNN, the INTSMC with T2FNN and the INTSMC system with PFNN is made in Table 1. It shows that the proposed INTSMC system with PFNN possesses the better tracking performance than others. The INTSMC with T2FNN shows a smaller error than the INTSMC system with PFNN; however, the former achieves this advantage at the cost of using the much more complex Karnik-Mendel iterative procedure for the type reduction operation.

Example 2: VCM actuator

The VCM actuator has many excellent features such as high-starting thrust force, high-speed operation, low cost and so on. The dynamics of the VCM actuator can be presented as (Seok and Kim, 2012; Wu et al., 2014)

$$\ddot{x} = f(\mathbf{x}) + g(\mathbf{x})u + d \tag{44}$$

where x is the position of the moving table, $\mathbf{x} = [x, \dot{x}]^T$ is the state vector, $f(\mathbf{x}) = \frac{-(K_t K_b + R_a B)}{(\overline{m} + M)R_a}\dot{x}$ is the system dynamic, $g(\mathbf{x}) = \frac{K_t}{(\overline{m} + M)R_a}$ is the control gain, $d = \frac{-F_f}{\overline{m} + M}$ is the external disturbance, u is the input voltage, R_a is the coil resistance, K_b is the back electromotive force coefficient, L_a is the coil inductance, M is the mass of the moving table, $\overline{m}$ is the mass of the payload, B is the viscous coefficient, K_t is the thrust force coefficient, i_a is the coil current, and F_f is the lumped friction force.

This paper proposes an experimental setup as shown in Fig. 9. The used 86duino platform is an open-source embedded platform based on Vortex86EX SoC and it can operate up to 400 MHz. On the software side, 86duino platform can support many x86 O/S as well as those running on the original Arduino base system. The control subroutine with 2 msec sampling rate is used for the execution of the control algorithms. Thereafter, the calculated

control effort is sent to the L298 motor driver. To investigate the robustness of the proposed INTSMC system, the system is tested under two different conditions. One is the nominal condition and the other is the payload condition by adding a payload on the moving table. The parameters of the INTSMC system are selected as $\lambda_1 = 0.5$, $p_1 = 7$, $q_1 = 5$, $\eta_\alpha = 10$, $\eta_c = \eta_l = \eta_r = \eta_\omega = \eta_h = 0.01$, $\mu_\alpha = \mu_c = \mu_l = \mu_r = \mu_\omega = \mu_h = 0.0001$, $K = 1$, $\rho = 0.2$, $\gamma = 1$, $E = 0.5$ and $\Phi = 1.0$. These parameters are selected through some trials.

For the comparison of the control performance, first, the PD control is applied to the VCM actuator. The PD control is given as $u_{pd} = 7.8e + 0.3\dot{e}$. All the gains are selected by trial-and-error to achieve the best control performance in the experimentation. The experimental results of the PD control are shown in Fig. 10. The experimental results show that the satisfactory performance is difficult to obtain for the PD control due to its linear structure with fixed control gains cannot cope with the uncertainties of the plant.

Then, the proposed ITSMC system with supervisory compensator (Chen and Hsu, 2010) is applied to the VCM actuator again and the corresponding experimental results are shown in Fig. 11. The experimental results show that favorable control performance can be achieved after learning of the parameters. However, the chattering phenomena are found due to the supervisory compensator with the bound of the approximation error $E = 2$ is used. The undesirable chattering control inputs will wear the mechanism and might excite unstable system dynamics. Further, the proposed ITSMC system with smooth compensator (Lin and Li, 2013) is applied to the VCM actuator again and the corresponding experimental results are shown in Fig. 12. The experimental results show that favorable control performance can be achieved without chattering problem for both of the test conditions. Though the control chattering has been eliminated by using the smooth compensator, the convergence speed of tacking error is slow.

Finally, the proposed ITSMC system with robust compensator is applied to the VCM

actuator again and the corresponding experimental results are shown in Fig. 13. The experimental results show that more favorable tracking performance with faster convergence speed of the tracking error can be obtained. Comparing with Figs. 11 and 12, the convergence speed of tracking error can speed up by the proposed robust compensator. In summary, a characteristic comparison between the PD control, the INTSMC system with supervisory compensator, the INTSMC system with smooth compensator and the INTSMC system with robust compensator is made in Table 2. It shows that the proposed robust compensator possesses the better tracking performance than others.

5. Conclusions

SMC system is one of the effective control methods since it is insensitive to parameter variations, external disturbance injection and fast dynamic response. In this paper, an INTSMC system via PFNN approach is proposed for an unknown nonlinear system. The proposed PFNN is a more generalized network with better learning ability and has lower computational complexity for practical implementation. In additional, Lyapunov stability theory is used to discuss the parameter learning and system stability of the INTSMC system. Finally, the effectiveness of the proposed INTSMC system has been confirmed by simulation and experimental results. In addition, the control performance of the proposed control scheme is robust with regard to external disturbances and parameter variations.

The main contributions of this paper are: (1) the PFNN can accurately approximate the unknown nonlinear term of control systems; (2) the perturbed asymmetric membership function not only can handle rule uncertainties but also the learning capability of the PFNN can be upgraded; (3) the INTSMC system can guarantee the tracking error convergence within a finite time; (4) the robust compensator not only can alleviate the control chattering but also can speed up the convergence speed of the tracking error; (5) the applicability of the

INTSMC system is demonstrated by an inverted pendulum and a VCM actuator.

Acknowledgments

The authors are grateful to the associate editor and the reviewers for their valuable comments. The authors appreciate the partial financial support from the Ministry of Science and Technology of Republic of China under Grant MOST 103-2221-E-032-063-MY2.

References

Abiyev, R.H., Kaynak, O., 2010. Type 2 fuzzy neural structure for identification and control of time-varying plants. IEEE Trans. Ind. Electr. 57, 4147–4159.

Castillo, O., Melin, P., 2012. A review on the design and optimization of interval type-2 fuzzy controllers. Appl. Soft Comput. 12, 1267–1278.

Chang, Y.H., Chan, W.S., 2014. Adaptive dynamic surface control for uncertain nonlinear systems with interval type-2 fuzzy neural networks. IEEE Trans. Cybern. 44, 293–304.

Chen, C.H., Hsu, C.F., 2010. Recurrent wavelet neural backstepping controller design with a smooth compensator. Neural Comput. Applic. 19, 1089–1100.

Chen, C.L., Chang, C.W., Yau, H.T., 2012. Terminal sliding mode control for aeroelastic systems. Nonlinear Dyn. 70, 2015–2026.

Chen, S.Y., Lin, F.J., 2011. Robust nonsingular terminal sliding-mode control for nonlinear magnetic bearing system. IEEE Trans. Control Syst. Technol. 19, 636–643.

Cheng, K.H., Hsu, C.F., Lin, C.M., Lee, T.T., Li, C., 2007. Fuzzy-neural sliding mode control for dc-dc converters using asymmetric Gaussian membership functions. IEEE Trans. Ind. Electron. 54, 1528–1536.

Feng, Y., Yu, X., Han, F., 2013. On nonsingular terminal sliding-mode control of nonlinear systems. Automatica 49, 1715–1722.

Gennaro, S.D., Domínguez, J.R., Meza, M.A., 2014. Sensorless high order sliding mode control of induction motors with core loss. IEEE Trans. Ind. Electr. 61, 2678–2689.

Hsu, C.F., 2012. Adaptive dynamic CMAC neural control of nonlinear chaotic systems with L_2 tracking performance. Eng. Appl. Artif. Intell. 25, 997–1008.

Hsu, C.F., Kuo, T.C., 2014. Intelligent complementary sliding-mode control with dead-zone parameter modification. Appl. Soft Comput. 23, 355–365.

Juang, C.F., Chen, C.Y., 2013. Data-driven interval type-2 neural fuzzy system with high learning accuracy and improved model interpretability. IEEE Trans. Cybern. 43, 1781–1795.

Juang, C.F., Chen, C.Y., 2014. An interval type-2 neural fuzzy chip with on-chip incremental learning ability for time-varying data sequence prediction and system control. IEEE Trans. Neural Netw. Learn. Syst. 25, 216–228.

Juang, C.F., Juang, K.J., 2013. Reduced interval type-2 neural fuzzy system using weighted bound-set boundary operation for computation speedup and chip implementation. IEEE Trans. Fuzzy Syst. 21, 477–491.

Karakose, M., 2010. Sine-square embedded fuzzy sets. 2010 IEEE International Conference on Syst. Man Cybern. 3628–3631.

Kayacan, E., Cigdem, O., Kaynak, O., 2012. Sliding mode control approach for online learning as applied to type-2 fuzzy neural networks and its experimental evaluation. IEEE Trans. Ind. Electr. 59, 3510–3520.

Kayacan, E., Kayacan, E., Khanesar, M.A., 2015. Identification of nonlinear dynamic systems using type-2 fuzzy neural networks-a novel learning algorithm and a comparative study. IEEE Trans. Ind. Electr. 62, 1716–1724.

Kim, N., Calise, A.J., 2007. Several extensions in methods for adaptive output feedback control. IEEE Trans. Neural Netw. 18, 482–494.

Komurcugil, H., 2013. Non-singular terminal sliding-mode control of DC–DC buck converters. Contr. Eng. Practice 21, 321–332.

Lee, L.W., Li, I.H., 2012. Wavelet-based adaptive sliding-mode control with H^{∞} tracking performance for pneumatic servo system position tracking control. IET Control Theory Appl. 6, 1699–1714.

Li, S., Zhou, M., Yu, X., 2013. Design and implementation of terminal sliding mode control method for PMSM speed regulation system. IEEE Trans. Ind. Inf. 9, 1879–1891.

Lin, C.K., 2006. Nonsingular terminal sliding mode control of robot manipulators using fuzzy wavelet networks. IEEE Trans. Fuzzy Syst. 14, 849–859.

Lin, C.M., Li, H.Y., 2013. Intelligent hybrid control system design for antilock braking systems using self-organizing function-link fuzzy cerebellar model articulation controller. IEEE Trans. Fuzzy Syst. 21, 1044–1055.

Lin, C.M., Li, H.Y., 2015. Dynamic Petri fuzzy cerebellar model articulation control system design for magnetic levitation system. IEEE Trans. Contr. Syst. Technol. 23, 693–699.

Lin, F.J., Chou, P.H., Chen, C.S., Lin, Y.S., 2012. Three-degree-of-freedom dynamic model-based intelligent nonsingular terminal sliding mode control for a gantry position stage. IEEE Trans. Fuzzy Syst. 20, 971–985.

Lin, F.J., Hung, Y.C., Hwang, J.C., Tsai, M.T., 2013. Fault-tolerant control of a six-phase motor drive system using a Takagi-Sugeno-Kang type fuzzy neural network with asymmetric membership function. IEEE Trans. Power Electron. 28, 3557–3572.

Lou, C.W., Dong, M.C., 2012. Modeling data uncertainty on electric load forecasting based on type-2 fuzzy logic set theory. Eng. Appl. Artif. Intell. 25, 1567–1576.

Mendel, J.M., 2001. Uncertain Rule-Based Fuzzy Logic System: Introduction and New Directions. Upper Saddle River, NJ, Prentice-Hall, 2001.

Mon, Y.J., Lin, C.M., 2012. Supervisory recurrent fuzzy neural network control for vehicle collision avoidance system design. Neural Comput. Applic. 21, 2163–2169.

Na, J., Ren, X., Zheng, D., 2013. Adaptive control for nonlinear pure-feedback systems with high-order sliding mode observer. IEEE Trans. Neural Netw. Learn. Syst. 24, 370–382.

Nayeripour, M., Narimani, M.R., Niknam, T., Jam, S., 2011. Design of sliding mode controller for UPFC to improve power oscillation damping. Appl. Soft Comput. 11, 4766–4772.

Seok, J.K., Kim, S.K., 2012. VCM controller design with enhanced disturbance decoupling for precise automated manufacturing processes. IET Electr. Power Appl. 6, 575–582.

Tan, C.P., Yu, X.H., Man, Z.H., 2010. Terminal sliding mode observers for a class of nonlinear systems. Automatica 46, 1401–1404.

Wang, L.X., 1994. Adaptive Fuzzy Systems and Control: Design and Stability Analysis. Englewood Cliffs, NJ: Prentice-Hall.

Wu, S., Jiao, Z., Yan, L., Zhang, R., Yu, J., Chen, C.Y., 2014. Development of a direct-drive servo valve with high-frequency voice coil motor and advanced digital controller. IEEE/ASME Trans. Mechatronics 19, 932–942.

Yang, J., Li, S., Su, J., Yu, X., 2013. Continuous nonsingular terminal sliding mode control for systems with mismatched disturbances. Automatica 49, 2287–2291.

Yang, J., Su, J., Lim S., Yu, X., 2014. High-order mismatched disturbance compensation for motion control systems via a continuous dynamic sliding-mode approach. IEEE Trans. Ind. Inf. 10, 604–614.

Yu, S., Yu, X., Shirinzadeh, B., Man, Z., 2005. Continuous finite-time control for robotic manipulators with terminal sliding mode. Automatica 41, 1957–1964.

Zhang, X., Sun, L., Zhao, K., Sun, L., 2014. Nonlinear speed control for PMSM system using sliding-mode control and disturbance compensation techniques. IEEE Trans. Power Electron. 28, 1358–1365.

Zhao, D., Li, C., Zhu, Q., 2011. Low-pass-filter-based position synchronization sliding mode control for multiple robotic manipulator systems. J. Syst. Control Eng. 225, 1136–1148.

Table 1. Performance measures for inverted pendulum example.

Methods	tracking error		
	maximum	average	standard deviation
dynamic fuzzy neural control	0.1227	0.0124	0.0155
INTSMC system with T1FNN	0.1567	0.0241	0.0300
INTSMC system with T2FNN	0.0602	0.0159	0.0123
INTSMC system with PFNN	0.0815	0.0174	0.0154

Table 2. Characteristic comparison.

Methods	stability proof	chattering phenomena	robustness	convergence speed
PD control	no	no	poor	slow
INTSMC system with supervisory compensator	yes	yes	excellent	fast
INTSMC system with smooth compensator	yes	no	middle	middle
INTSMC system with robust compensator	yes	no	excellent	fast

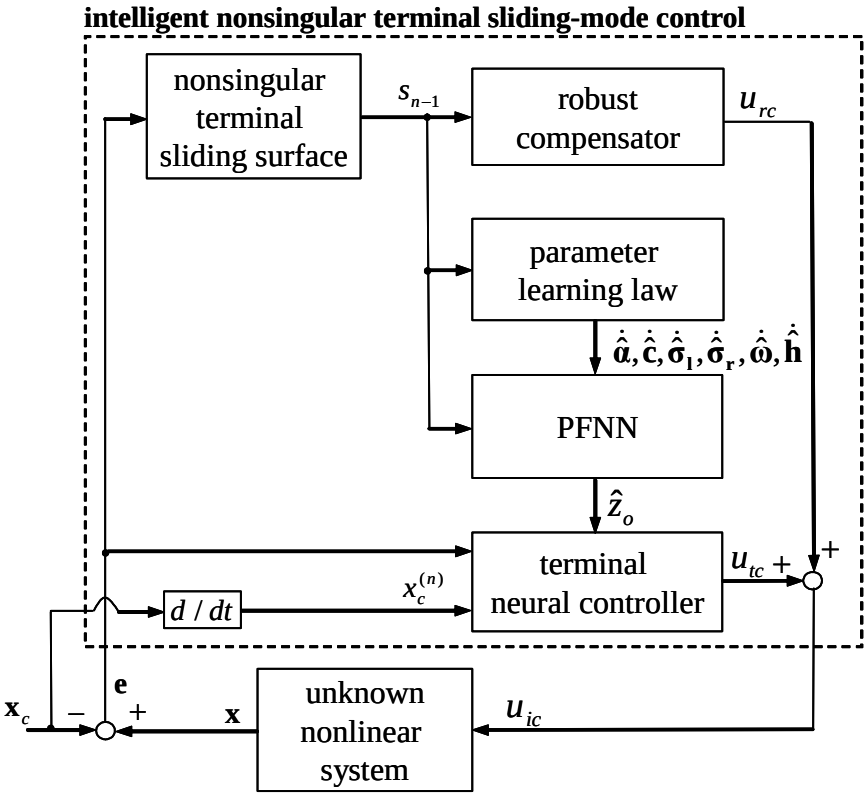

Fig. 1. The block diagram of the proposed INTSMC system.

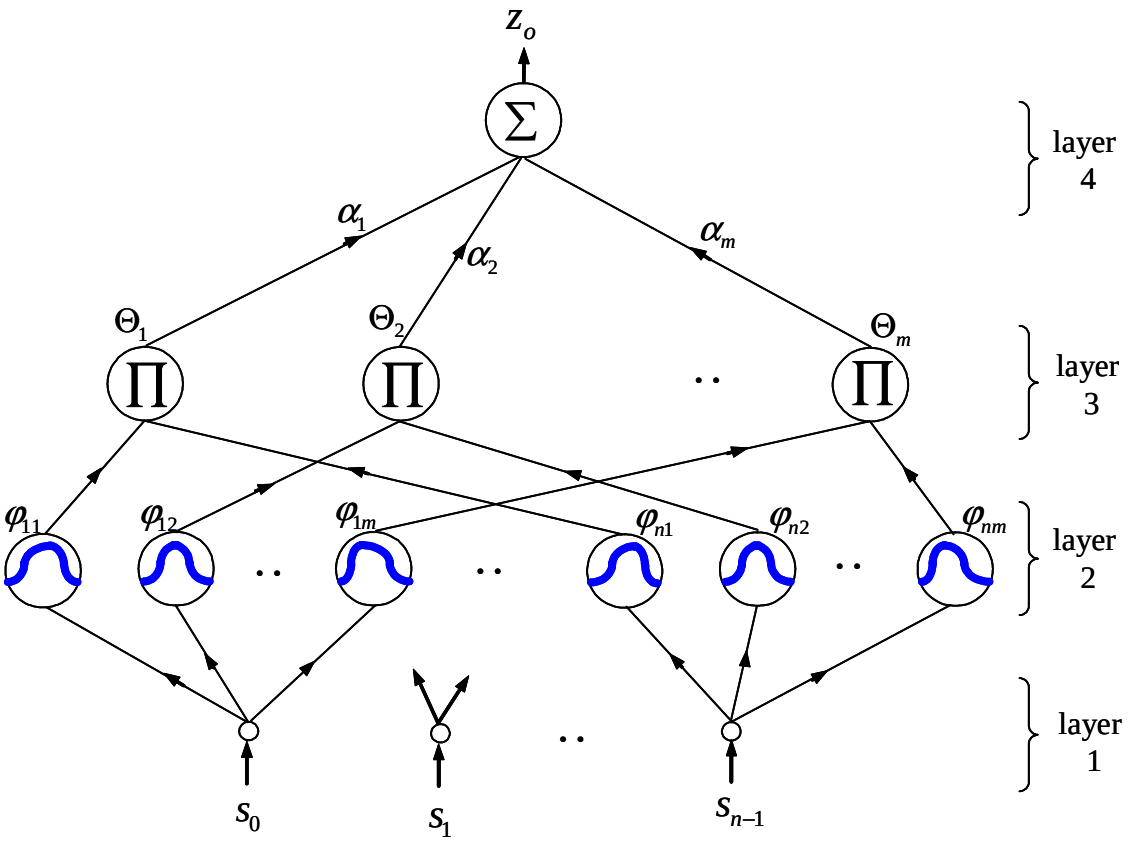

Fig. 2. Network structure of PFNN.

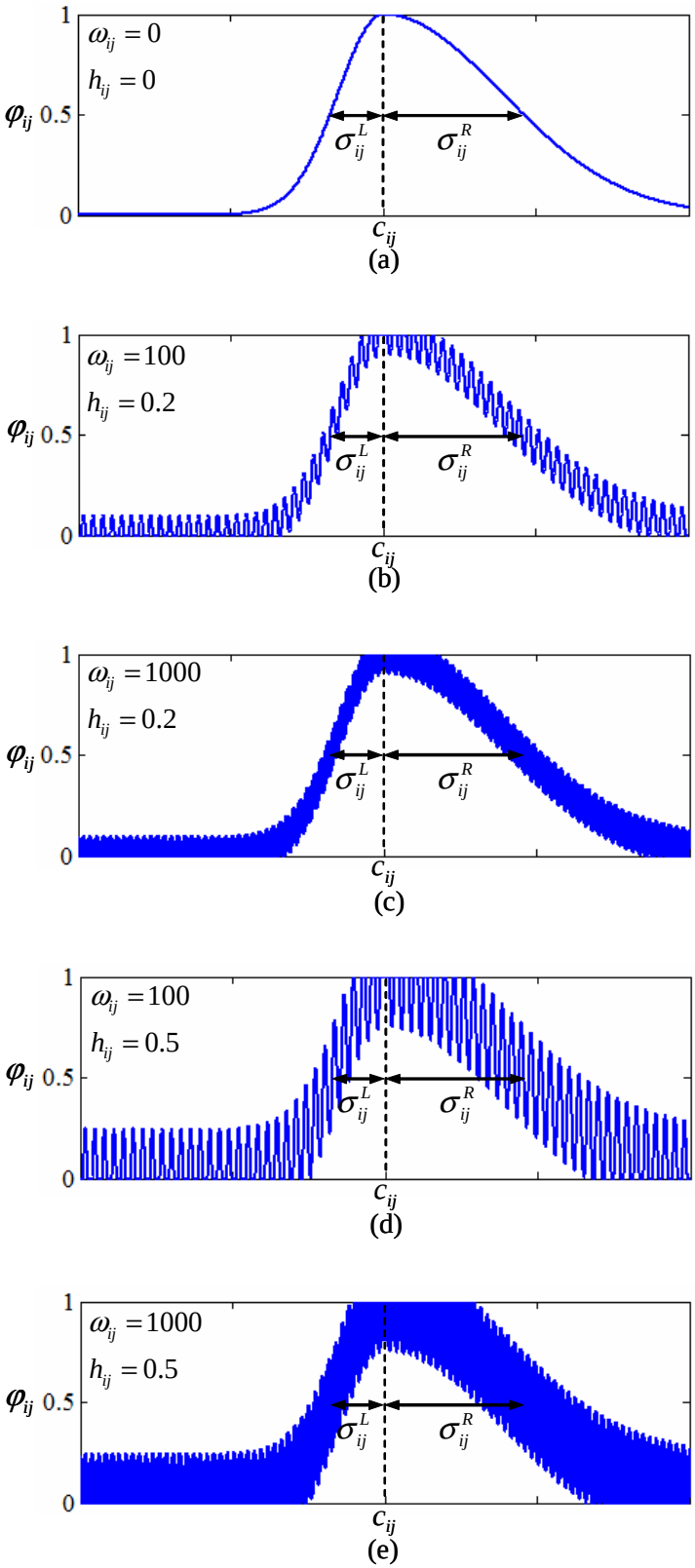

Fig. 3 Perturbed asymmetric membership function with different perturbations.

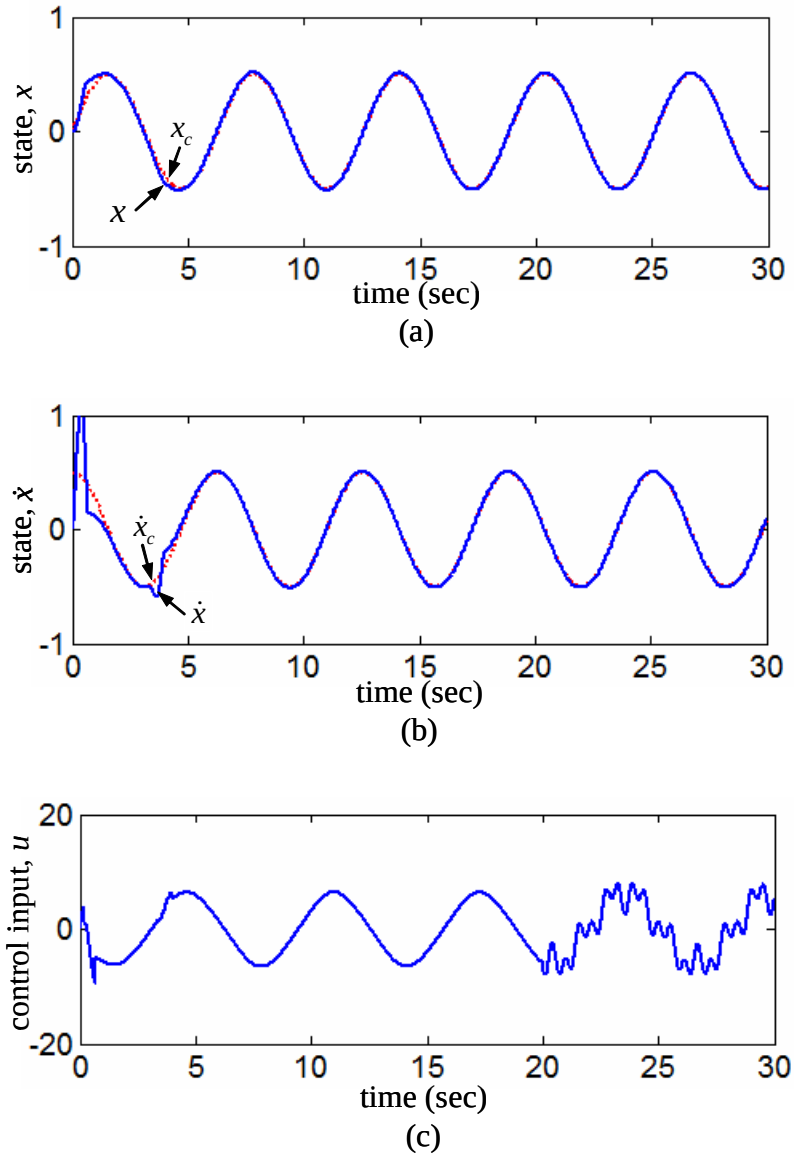

Fig. 4 Simulation results of the dynamic fuzzy neural control for inverted pendulum.

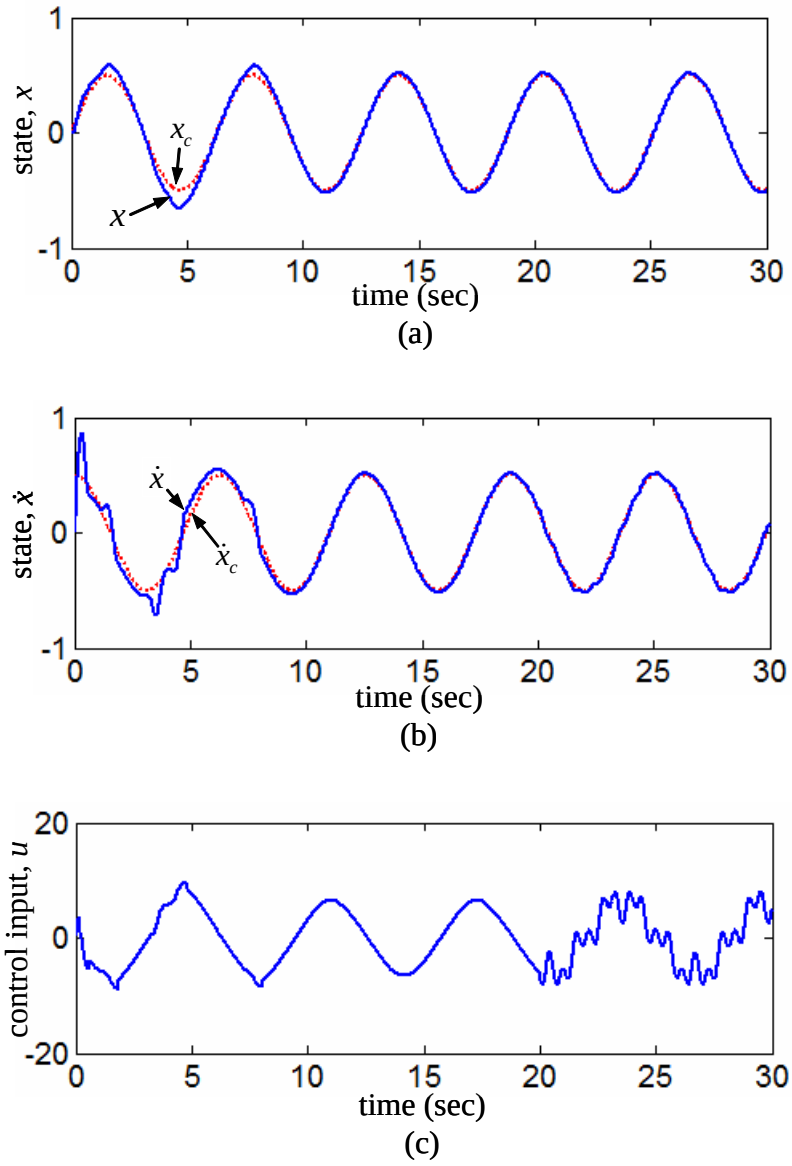

Fig. 5 Simulation results of the INTSMC system with T1FNN for inverted pendulum.

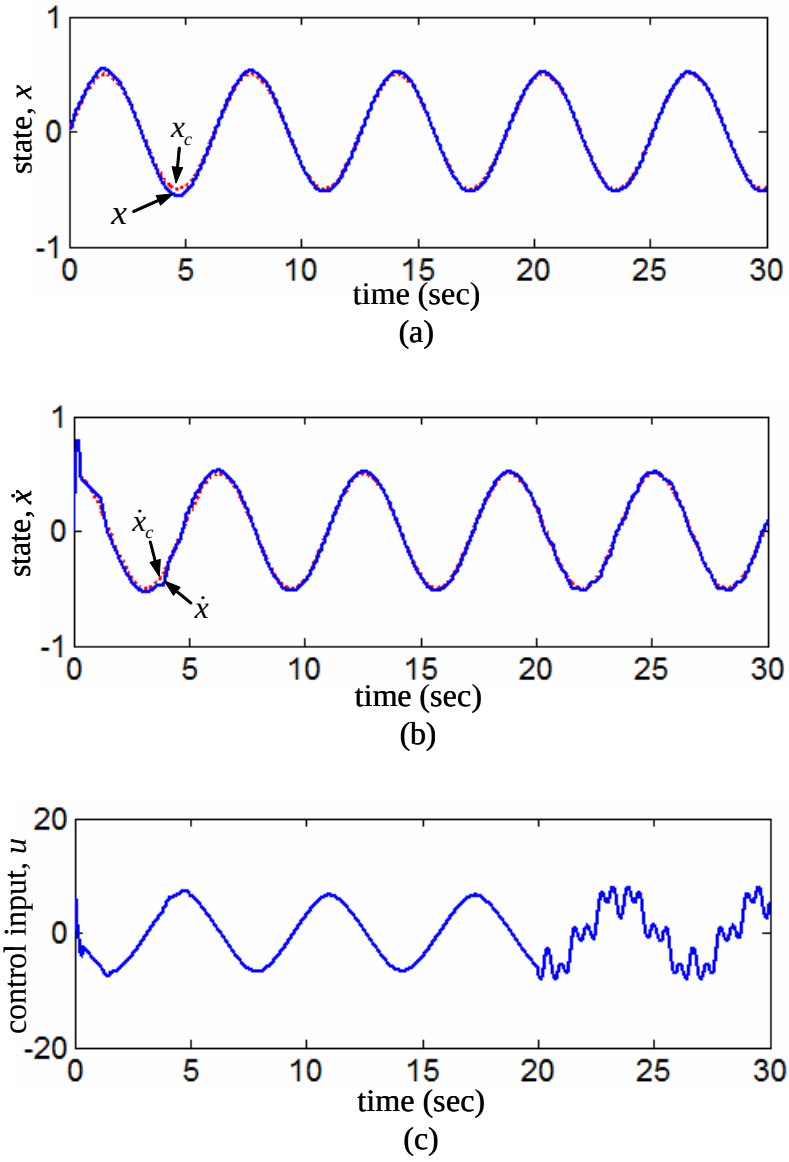

Fig. 6 Simulation results of the INTSMC system with T2FNN for inverted pendulum.

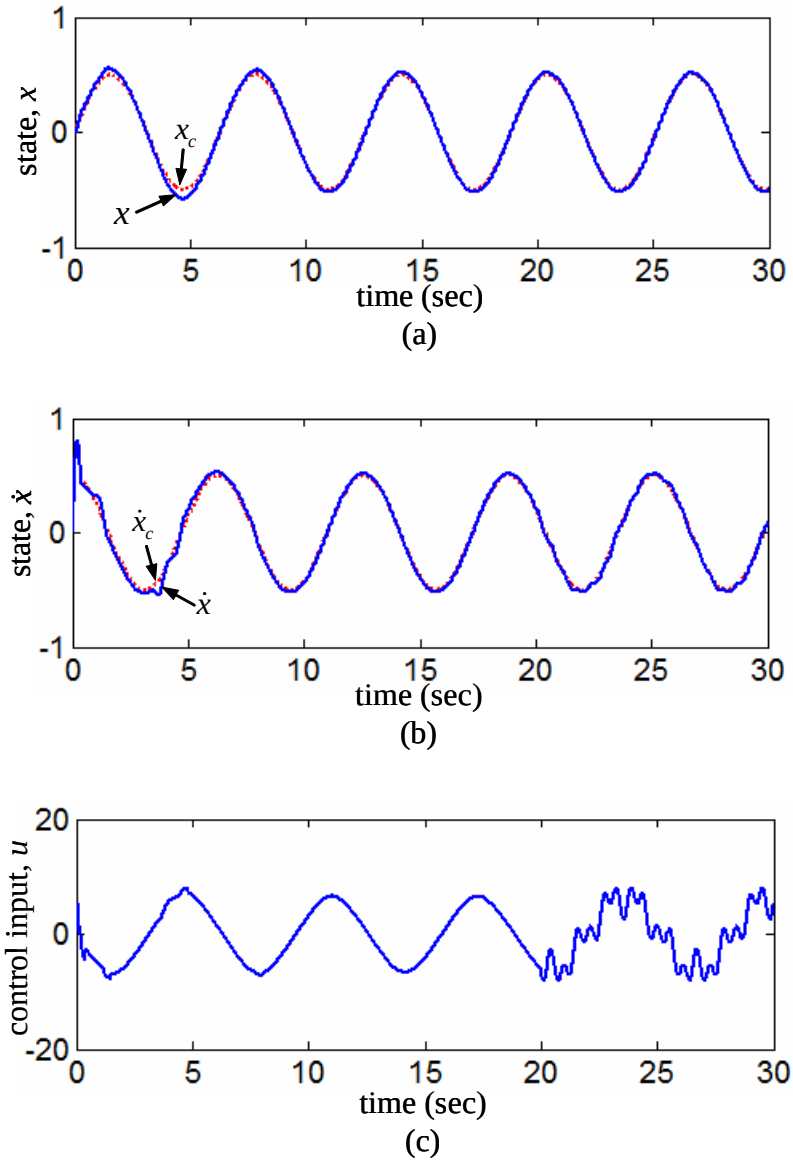

Fig. 7 Simulation results of the INTSMC system with PFNN for inverted pendulum.

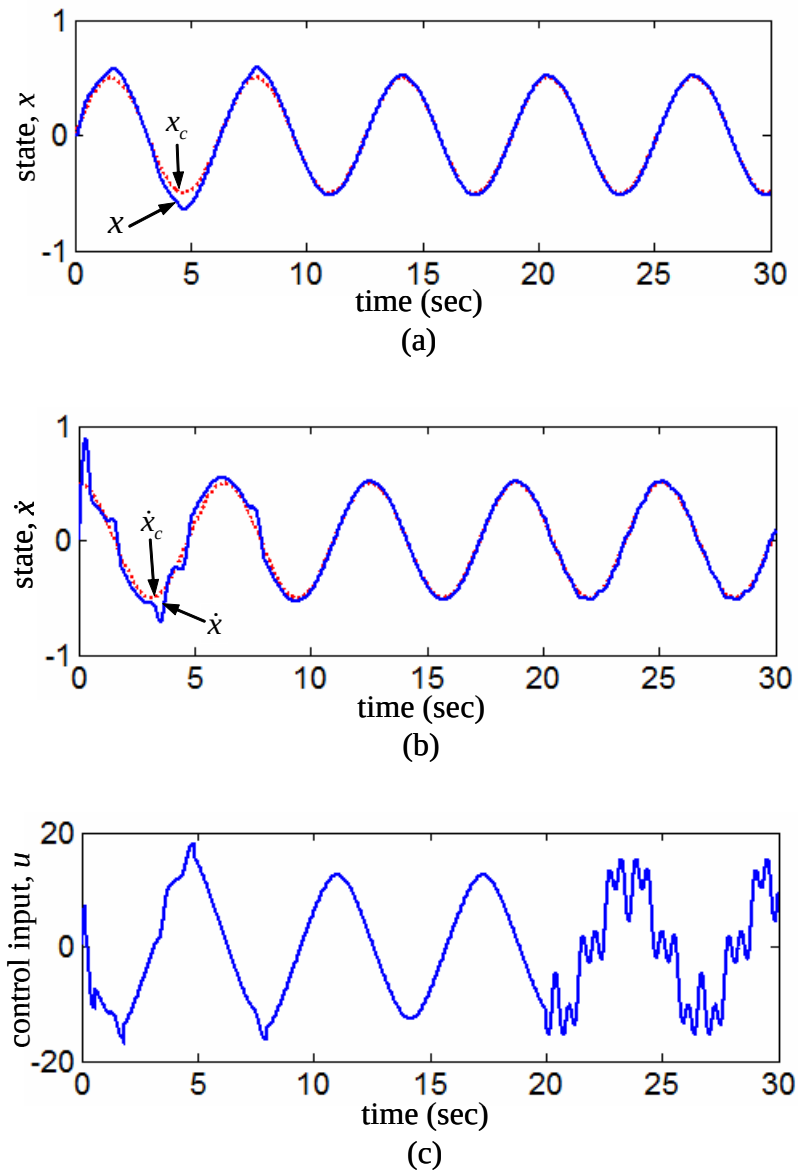

Fig. 8 Simulation results of the INTSMC system with PFNN under parameter variations.

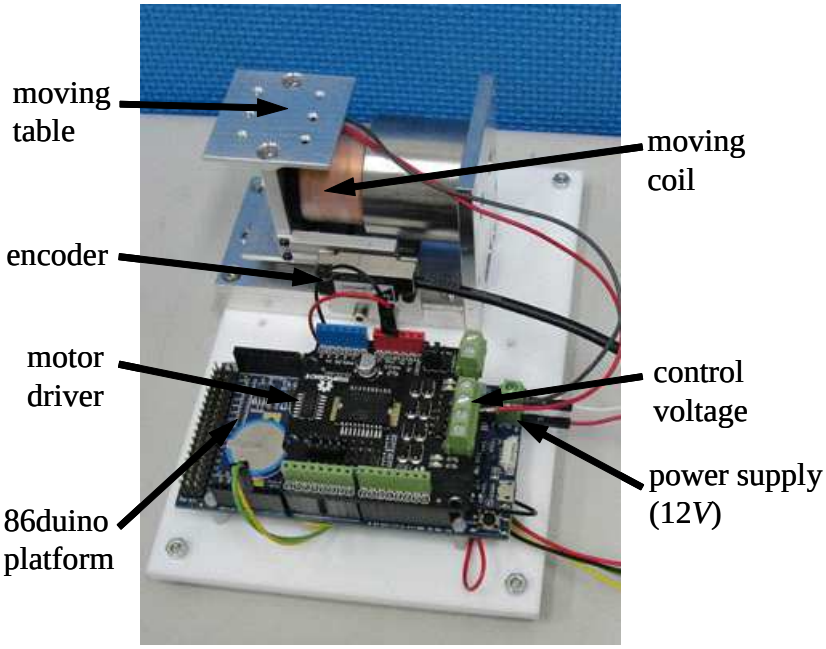

Fig. 9 Experimental setup of VCM actuator.

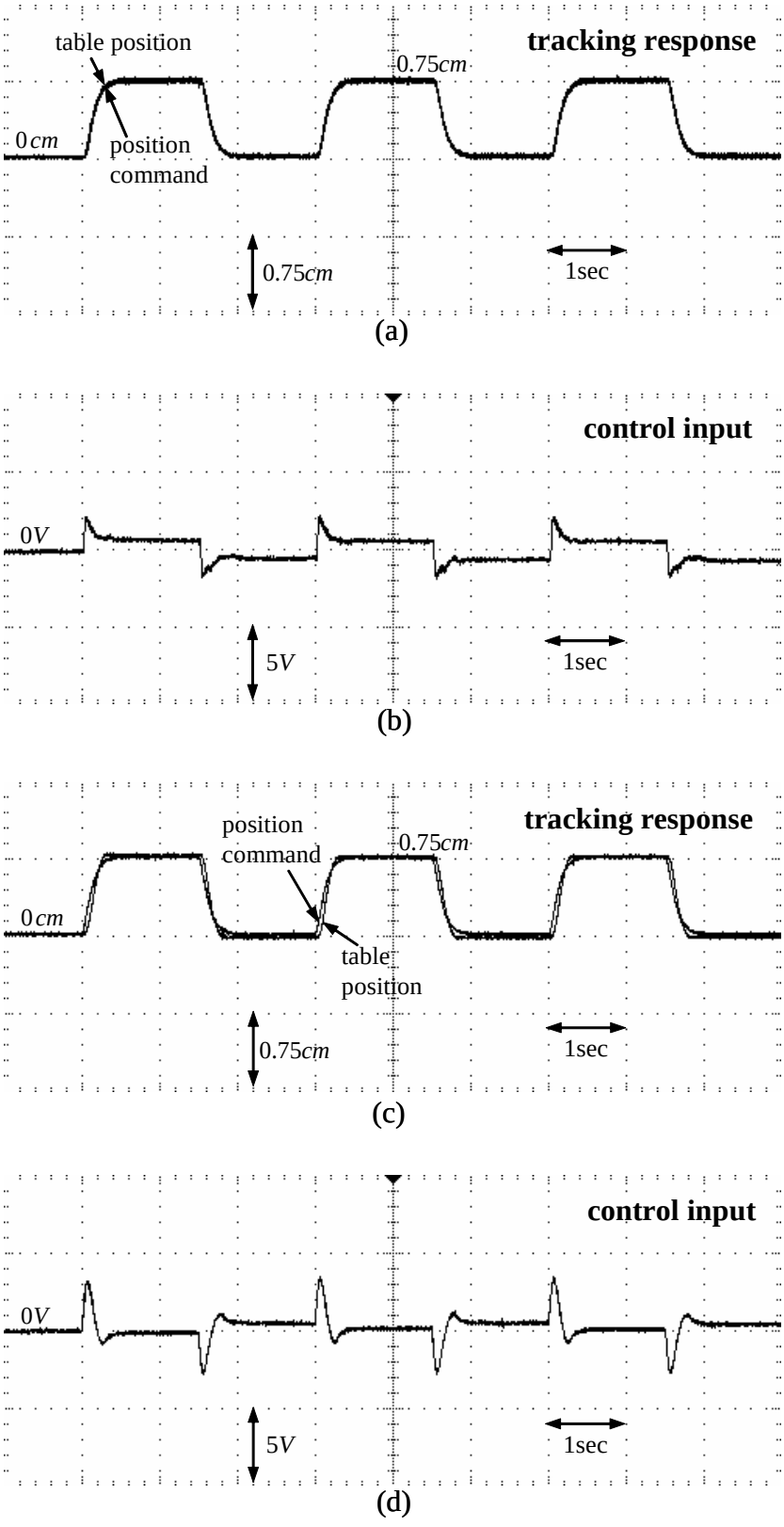

Fig. 10 Experimental results of the PD control for VCM actuator.

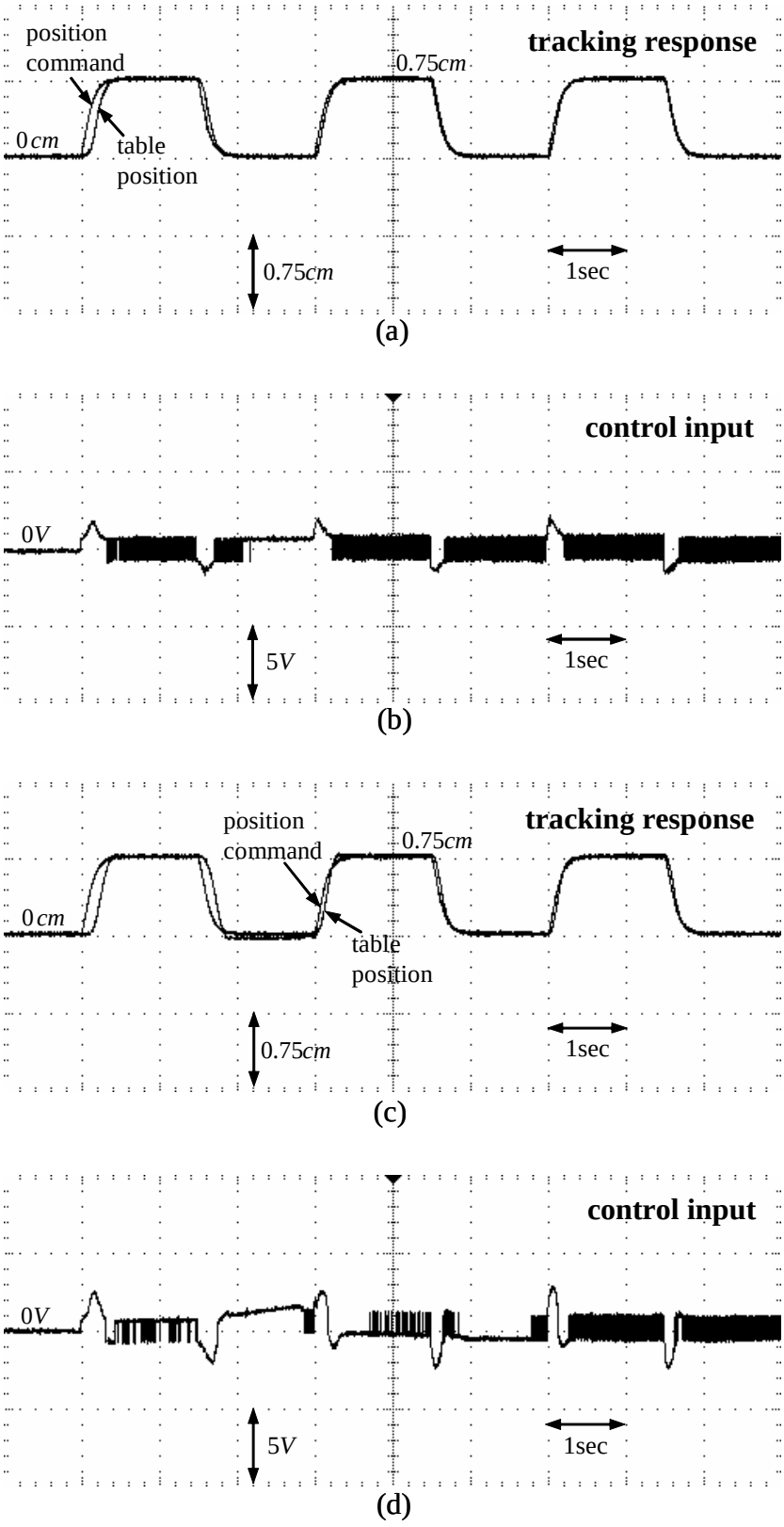

Fig. 11 Experimental results of the INTSMC system with supervisory compensator for VCM actuator.

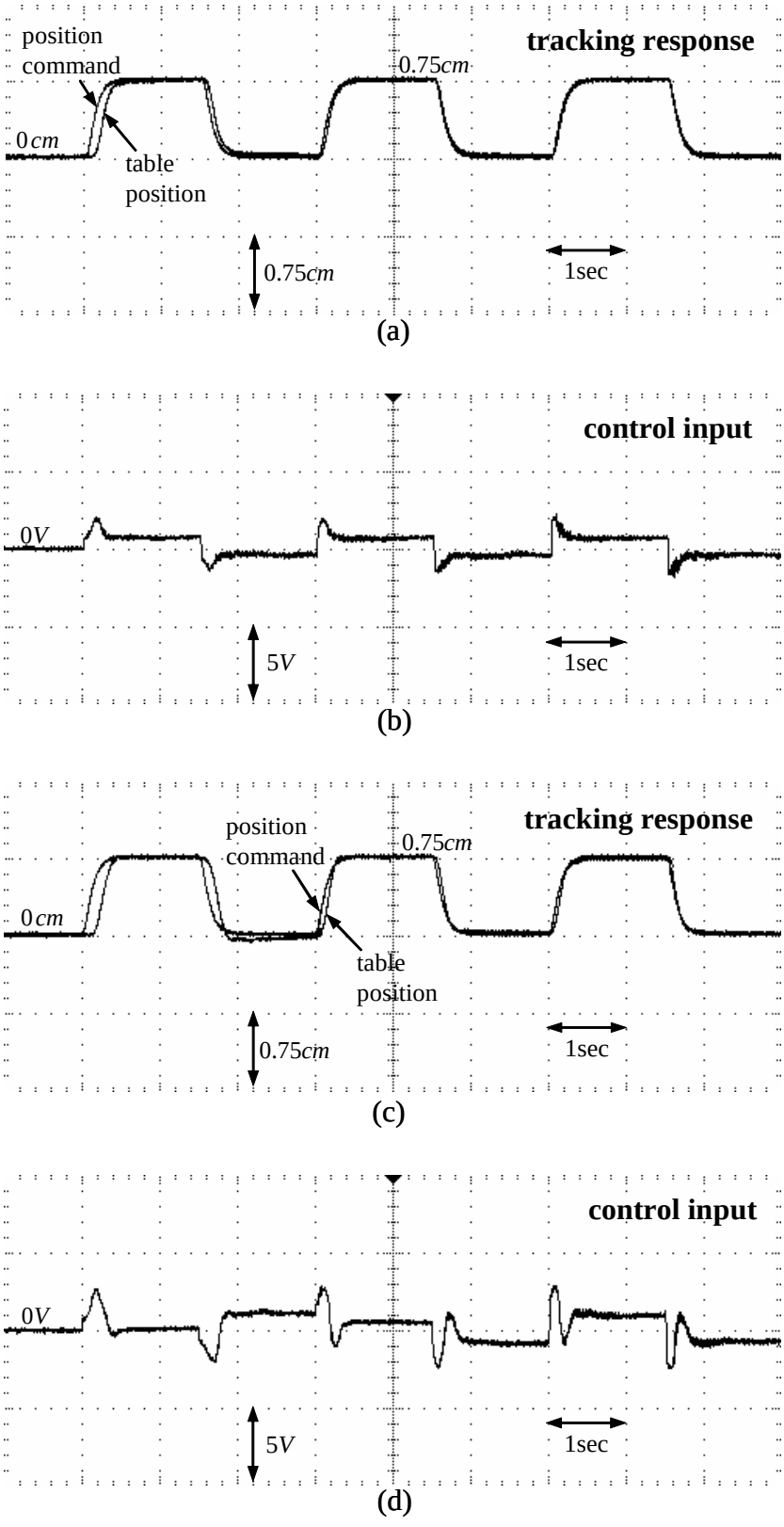

Fig. 12 Experimental results of the INTSMC system with smooth compensator for VCM actuator.

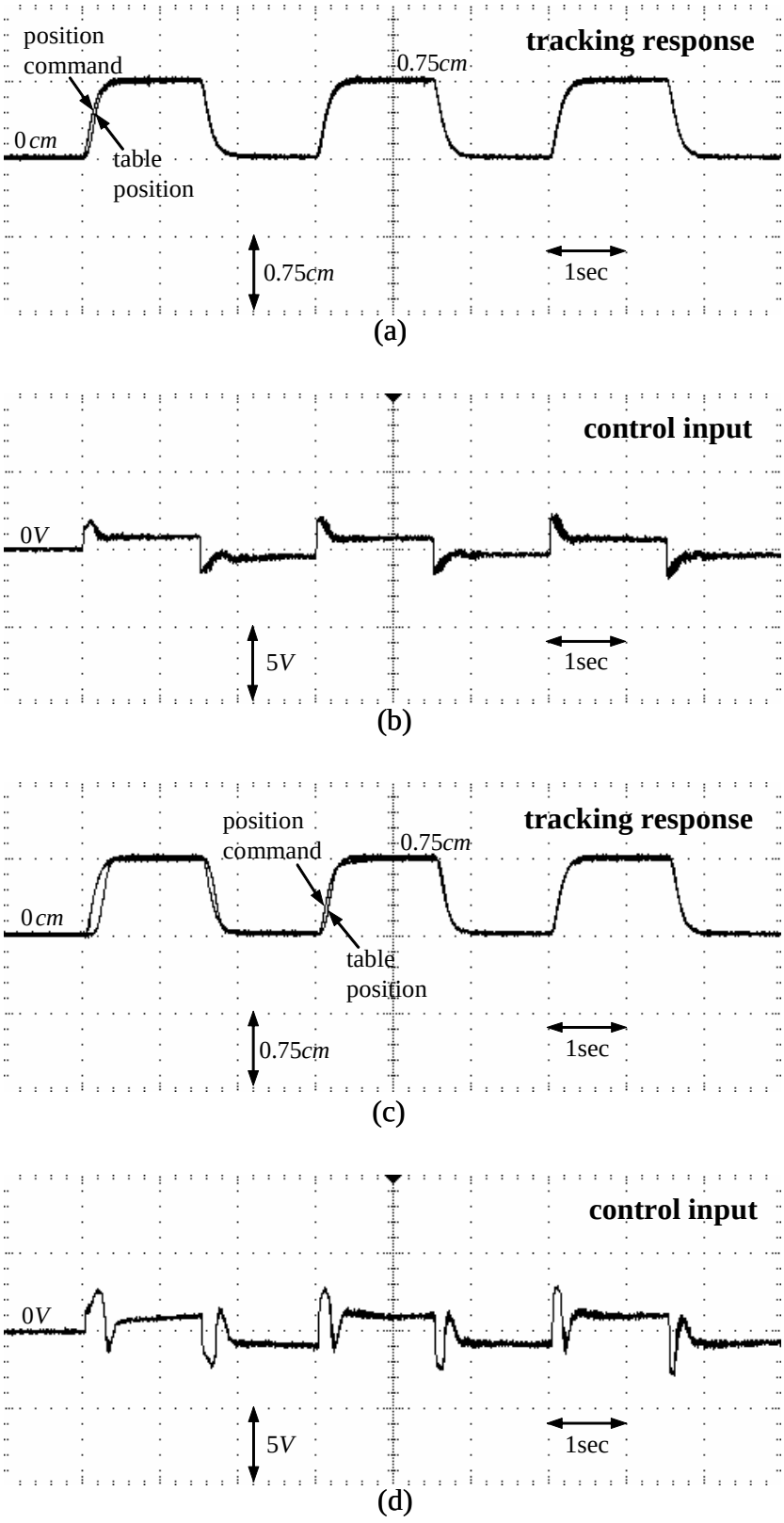

Fig. 13 Experimental results of the INTSMC system with robust compensator for VCM actuator.